Nucleation rate data using a continuous adiabatic expansion of a gas/vapor mixture at high pressures

van Eeghem, R.A.J.

Award date:
1995

Technische Universiteit tu Eindhoven

Vakgroep Transportfysica
Faculteit Technische
Natuurkunde
Gebouw W&S
Postbus 513
5600 MB Eindhoven

Titel: Nucleation rate data using a continuous adiabatic expansion of a gas/vapor mixture at high pressures.

Auteur: R.A.J. van Eeghem

Verslagnummer: R - 1357 - A

Datum: 22 Augustus 1995

Werkeenheid: Gasdynamica/Aeroakoestiek

Begeleider(s): Prof. dr. ir. M.E.H. van Dongen
Ir. M.J.E.H. Muitjens

"To Astrid, for her support"
- Ruud -

PREFACE

The process of dropletwise homogeneous condensation can be used to separate two gaseous substances. It is a combined process of droplet formation, called *nucleation,* and droplet growth. Our interest is focused to the formation of droplets, called nucleation, and the effect of pressure on nucleation. The process of nucleation is studied using an expansion cloud chamber in combination with the measurement of the extinction of light. Via a numerical simulation of the expansion cloud chamber, the effect of surface tension, diffusion coefficient, initial vapor pressure and initial temperature on the extinction signal is examined. The same numerical simulation is used in the analysis of these experiments using two nucleation theories: the classical nucleation theory and the semi-phenomenological theory. This yields a correction value Γ for the theoretical nucleation rate. These values of Γ are presented against the values found in the literature.

TABLE OF CONTENTS

INTRODUCTION

Dropletwise condensation is the process of a vapor turning into liquid droplets. It's an important process. Without it, for example, rain would never exist. But also numerous industrial processes use dropletwise condensation. One could, for instance, think of a way to separate a mixture of different gases. If the condensation of each gas occurs at a different thermodynamic state then it is possible to separate them.

To observe condensation, a vapor has to be brought into a thermodynamic state in which the liquid phase is favorable above the gaseous phase (a gas having pressure and temperature below the critical point is referred to as a vapor). This procedure is shown in figure 1 (dotted line), where a pT-diagram of an arbitrary gas is shown. The vapor starts at an initial thermodynamic state (p_i,T_i) somewhere in the gas region and is then brought into a state (p_f,T_f) somewhere in the liquid region.

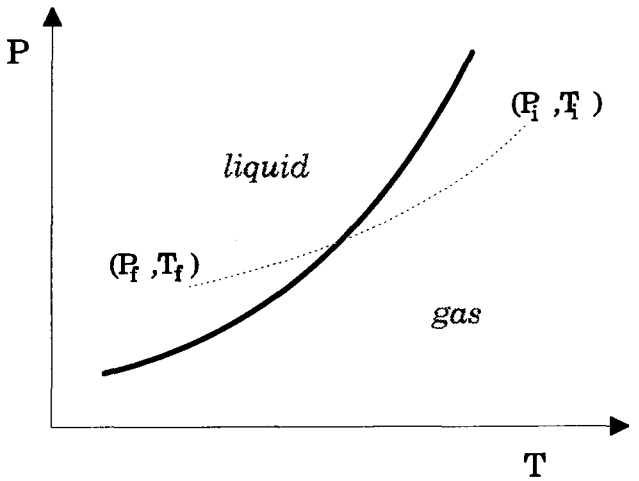

Figure 1 : pT-diagram of an arbitrary gas in the region of interest

An important parameter in this process is the *saturation ratio* S, defined as the ratio of the current vapor pressure p_v and the equilibrium vapor pressure $p_{v,sat}$ above a liquid plane at the same temperature T.

$$S = \left.\frac{p_v}{p_{v,sat}}\right|_T \tag{1.1}$$

The vapor is called *undersaturated* if S<1, indicating that the thermodynamic state of the vapor is in the gas region. The vapor is called *saturated* if the thermodynamic state of the vapor is at the equilibrium line or S=1. The *supersaturated* state occurs for S>1, indicating that the thermodynamic state of the vapor is in the liquid region.

If, for a pure vapor, the conditions for condensation are favorable then liquid will be formed. In the vicinity of a surface (e.g. borders, dust particles), this liquid will always be formed on the surface. This process is called *heteroge-*

neous condensation. In the absence of a surface however, droplets will be formed out of vapor molecules. This process is called *homogeneous condensation*.

In case of homogeneous condensation, the molecules forming the droplet also have to create a surface. Since the formation of a surface always costs energy the formation of droplets, in the case of homogeneous condensation, is a constraint process. This means that there is an energy barrier involved that has to be passed before droplets can be created. It is this energy barrier that will prevent condensation of a vapor in the saturated state. Instead the first droplets are formed at a thermodynamic state deep into the liquid region.

This report is devoted to the study of *homogeneous nucleation*, that is the formation of droplets in pure gases in the absence of a condensation surface. Our interest is particular focused at the effect of carrier gas pressure at nucleation rates (the so called *Pointing effect*). The experiments are part of a larger study of nucleation in carbon-hydrogen mixtures at high pressures.

The theoretical description of nucleation is presented in the next chapter (chapter 2), describing two nucleation models, the *classical nucleation theory* (CNT) and the *semi-phenomenological theory* (SPT). The classical nucleation theory assumes that the vapor can be described using the ideal gas law and that the liquid formed is incompressible. This in contrast to the semi-phenomenological theory, which uses a non-ideal description of the vapor phase.

In chapter 3 a numerical simulation of the homogeneous condensation process in a gas/vapor mixture is presented, using either the CNT or SPT in combination with the droplet growth model of Gyarmathy. This simulation is then used to analyze the sensitivity of the condensation process to changes in the descriptive parameters (e.g. surface tension, diffusion coefficient, vapor pressure).

In order to create conditions that are favorable for condensation, the vapor has to be brought from an initially undersaturated state to a supersaturated state. This state can be created by various experimental techniques. One method is the shock-tube[1], another method used is the expansion cloud-chamber. The latter one uses a continuous adiabatic expansion to create a rapid change in both pressure and temperature. The experimental results presented in this report are acquired using the expansion cloud chamber, which is covered in more detail in chapter 4. In the last paragraph of this chapter the numerical simulation of chapter 3 is used to analyze the measurements yielding a correction factor for the theoretical nucleation rate called Γ.

[1] An interesting modification of the use of a shock tube in the study of condensation is described by Looijmans [LOO95]

THEORY OF NUCLEATION

2.1 Introduction

Homogeneous condensation in the absence of a surface can be separated into two physically distinct processes. The formation of the droplets or *nucleation* and the *droplet growth*. As mentioned in the previous chapter, the nucleation is a constraint process that involves an energy barrier. This energy barrier will prevent instantaneous nucleation if the thermodynamic state of the gas enters the liquid region. Instead the nucleation has its onset at a thermodynamic point somewhere in the liquid region, called the *Wilson point*. Theoretical descriptions of nucleation differ mostly in the description of the energy barrier.

2.2 Energy barrier of a n-cluster

The basic assumption of a nucleation theory is that a small droplet can be considered a cluster of molecules. From this point of view a logical starting point is the process of the clustering of vapor molecules. Consider a vapor containing only single molecules (called *1-clusters* or *monomers*). These molecules will have kinetic energy and thus they have a probability to collide with other molecules. During this collision (assuming it is inelastic) there is a chance that the molecules will form a bound, that is, they will form a 2-cluster or *dimer*. The same process can be repeated for dimers yielding *3-clusters* or *trimers*, for trimers yielding 4-clusters etc. On the other hand, a cluster can also lose a molecule. So in equilibrium a distribution of *n-clusters* will be formed (a n-cluster is a closely tied group of n vapor molecules). This equilibrium distribution is described by the well known Boltzmann expression:

$$n_n = n_1 e^{-\Delta G_n / k_B T} . \qquad (2.1)$$

In (2.1) n_n denotes the number of clusters containing n molecules, n_1 is the number of monomers, k_B is the Boltzmann factor, T the temperature and $\Delta G(n)$ is the Gibbs free energy needed to create a n-cluster from n monomers. From (2.1) the *number density of n-clusters* ρ_n can easily be found by expressing (2.1) per unit of volume.

From (2.1) it is clear that the value of n_n is dominated by the value $\Delta G(n)/k_B T$, where the actual value of $\Delta G(n)$ is depending on the model used to describe the energy of formation of a n-cluster. Different nucleation theories use a different description for $\Delta G(n)$. Nevertheless, in most theories, $\Delta G(n)$ contains

a volume term and a surface term:

$$\Delta G(n) = c_{vol} n + c_{surf} n^{2/3} . \qquad (2.2)$$

The surface term $c_{surf} \cdot n^{2/3}$ describes the energy needed to create a surface for a cluster of n molecules. It is always positive since it costs energy to create a surface. The corresponding constant c_{surf} depends on the macroscopic surface tension γ.

The volume term $c_{vol} \cdot n$ describes the energy gained by the clustering of n molecules. It can be either positive or negative. In the gas region, the gaseous phase is energetically in favor above the liquid phase, so the clustering of molecules will cost energy and $c_{vol} \cdot n$ will be positive. If the thermodynamic state is in the liquid region, the opposite is true and $c_{vol} \cdot n$ will be negative. It is then clear from (2.2) that $\Delta G(n)$ contains an extremum. The constant c_{vol} depends on the saturation ratio S. In figure 2 a plot is given of $\Delta G(n)$ as a function of the cluster size. It shows that for supersaturated states there is a maximum in $\Delta G(n)$. The cluster size n^* at this maximum is called the *critical cluster size* and is denoted by n^*. It can be found by solving (2.3). The corresponding value of $\Delta G(n)$ is denoted by $\Delta G(n^*)$.

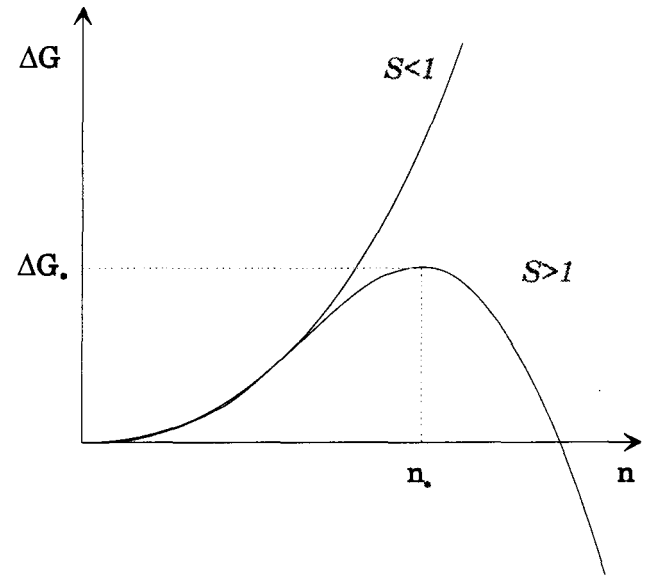

Figure 2 : plot of ΔG(n) versus n for the undersaturated (S<1) and the supersaturated (S>1) state

$$\left(\frac{\partial \Delta G(n)}{\partial n} \right)_{p,T} = 0 \qquad (2.3)$$

Now a critical cluster can interact with a monomer and form a cluster of size n^*+1. From figure 2 it can be seen that for any cluster larger than size n^*, the slope of $\Delta G(n)$ is negative and the addition of molecules releases energy whereas the loss of a molecule will cost energy. So once a cluster has reached a size larger than the critical clustersize n^* it is energetically favorable to grow to macroscopic sizes. On the other hand, if a cluster of size n^* releases a molecule

it will evaporate because it will lose energy by releasing even more vapor molecules. So the number of droplets eventually formed per unit of time and per unit of volume, the so called *nucleation rate*, will be highly dependant on the number of critical clusters per unit of volume.

Now assume, in a first approximation, that the number of critical clusters is given by the Boltzmann expression. Then the nucleation rate can be written as

$$J(n) = J(0)e^{-\Delta G(n^*)/k_B T} . \qquad (2.4)$$

Here the kinetic prefactor J(0) contains the number of monomers times the collision frequency (assuming each collision yields the addition of a molecule). Since the process of nucleation is a non-equilibrium process the Boltzmann expression cannot be used. However it will turn out that (2.4) will be the general form of the nucleation rate. Any nucleation theory will, in general, face two problems. How to describe the energy barrier $\Delta G(n)$ and how to describe the kinetic prefactor J(0).

2.3 Basic kinetics of nucleation and the classical nucleation theory

From the above it is clear that the actual formation of droplets is a kinetic process. More important, it is a non-equilibrium process. Since the Boltzmann expression describes an equilibrium distribution it is clear that the number of critical clusters cannot be given by the Boltzmann expression.

The Gibbs free energy for a vapor in supersaturated state plotted against the density, shown in figure 3, contains two minima. A local minimum describing the supersaturated vapor and a global minima describing the thermo-dynamically stable liquid state. The number distribution of n-clusters in the metastable equilibrium state (the local minimum) is given by the Boltzmann expression. The idea is now to express the non-equilibrium

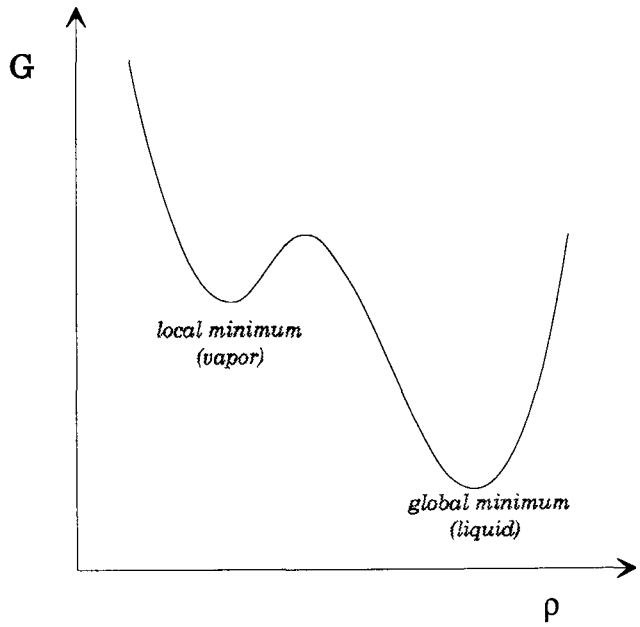

Figure 3 : G versus the overall density ρ for arbitrary (p,T) somewhere in the liquid region.

density of n-clusters $\rho(n)$ in terms of the equilibrium density of n-clusters $\rho_{equ}(n)$.

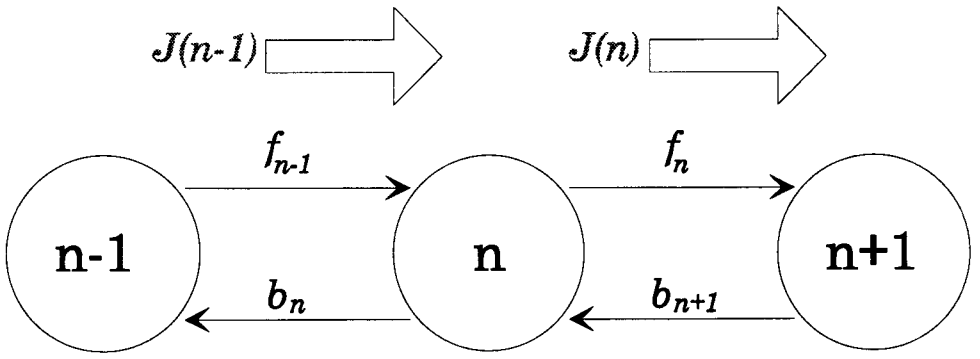

Figure 4 : The kinetic process of nucleation.

The change in the number density of n-clusters contains two fluxes. The number of (n-1)-clusters capable of growing to a n-cluster (the n-1 nucleation rate or J(n-1)) minus the number of n-clusters capable of growing to a size n+1 (the n nucleation rate or J(n)). So the change in $\rho(n,t)$ is given by

$$\frac{\partial \rho(n,t)}{\partial t} = J(n-1) - J(n) . \tag{2.5}$$

The nucleation rate of n-clusters J(n) can again be split into two different processes (as shown in figure 4)

$$J(n) = f_n \rho(n,t) - b_{n+1} \rho(n+1,t) . \tag{2.6}$$

Assuming only monomer addition and substraction then the first term on the r.h.s. of equation (2.6) describes the number of n-clusters growing to size n+1 (the *forward rate*) and the second term on the r.h.s. describes the number of (n+1)-clusters "decaying" to an n-cluster (the *backward rate*). The factor f_n can be found using the gas kinetic formula [LAN69] and the definition of the surface of a n-cluster s_n,

$$f_n = \theta \nu s_n = \frac{\theta p_v s_n}{(2\pi m_1 k_B T)^{1/2}} , \tag{2.7}$$

$$s_n = s_1 n^{2/3} = (36\pi)^{1/3} (v_{liq})^{2/3} \cdot n^{2/3} .$$

Here v_{liq} is the liquid molecular volume, p_v the partial vapor pressure, m_1 the molecular mass and θ is the *mass accommodation coefficient*, describing the chance that a collision yields the addition of a monomer. Literature values of θ range from 0.1 to 1 [ABR74]. In our case it is set to unity, implying that each collision yields the addition of a monomer.

Now assume the clustersize n is large. Then the addition or substraction of a monomer is only a small change, compared to the size of the cluster. So quantities depending on the clustersize n can be considered continuous in n. As a consequence of this, the change of a quantity as the clustersize changes from n to n+1 can be approximated by the first derivative, so:

$$\begin{aligned} \rho(n+1,t) - \rho(n,t) &\approx \frac{\partial \rho(n,t)}{\partial n}, \\ \Delta G(n+1) - \Delta G(n) &\approx \frac{\partial \Delta G(n)}{\partial n}, \\ J(n+1) - J(n) &\approx \frac{\partial J(n)}{\partial n}. \end{aligned} \tag{2.8}$$

Using (2.8), the kinetic equation (2.5) can be rewritten to

$$\frac{\partial \rho(n,t)}{\partial t} = -\frac{\partial J(n)}{\partial n}. \tag{2.9}$$

At the metastable equilibrium in figure 3, the net nucleation rate is zero, so a relation for the coefficient b_{n+1} of the backward rate is found:

$$b_{n+1} = f_n \frac{\rho_{equ}(n)}{\rho_{equ}(n+1)}. \tag{2.10}$$

Using for $\rho_{equ}(n)$ the Boltzmann expression and linearizing $\rho_{equ}(n)/\rho_{equ}(n+1)$, equation (2.10) can be simplified to

$$b_{n+1} \approx f_n \left(1 + \frac{\partial}{\partial n} \left[\frac{\Delta G(n)}{k_B T} \right] \right). \tag{2.11}$$

With the approximation (2.8) and neglecting the second order terms, the relation for J(n) in non-equilibrium now becomes

$$J_n = -B\frac{\partial \rho(n,t)}{\partial n} + A\,\rho(n,t)\,,$$
$$B = f_n, \qquad A = -f_n \cdot \frac{\partial}{\partial n}\left[\frac{\Delta G(n)}{k_B T}\right]. \tag{2.12}$$

This is the so called Fokker-Planck equation, where B is a diffusion coefficient describing the diffusion in the space of clustersizes and A is the drift coefficient. The function $\Delta G(n)$ can be seen as the potential driving the diffusion in the space of clustersizes.

The coefficient A can be expressed in terms of $\rho(n,t)/\rho_{equ}(n)$, using the Boltzmann expression for $\rho_{equ}(n)$ and computing the derivative of $\rho_{equ}(n)$ with respect to n. As a result equation (2.12) can now be rewritten to

$$J_n = -f_n \rho_{equ} \frac{\partial}{\partial n}\left[\frac{\rho(n,t)}{\rho_{equ}(n)}\right]. \tag{2.13}$$

The solution of equation (2.9) yields a time dependant nucleation rate J(n,t). This nucleation rate, however, rapidly converges to a time independent solution, the so called *steady state nucleation rate* or $J_{ss}(n)$[1]. The characteristic time at which the nucleation rate converges to the steady state solution is given by [ABR74]

$$\tau_{ss} = \frac{1}{4\pi f_n \cdot Z^2}\,, \tag{2.14}$$

where f_n^* is the forward rate for critical clusters and Z the Zeldovich factor. Now for the experiments, discussed in chapter 4 of this report, the value of τ_{ss} is in the order of μs, , whereas the timescale of the experiment is in the order of ms. So only a small error is introduced if the steady state nucleation rate $J_{ss}(n)$ is used instead of the time dependent nucleation rate J(n,t). Using $J_{ss}(n)$ and the

[1] Note that $J_{ss}(n) \equiv J(n)$.

steady state solution of the number density of n-clusters $\rho_{ss}(n)$ the value of $\rho_{ss}(n)/\rho_{equ}(n)$ can be found by integration of (2.13),

$$\frac{\rho_{ss}(n)}{\rho_{equ}(n)} = -J_{ss}(n)\int_1^n \frac{dn}{f_n \rho_{equ}(n)} + \text{const} . \tag{2.15}$$

To obtain the value of the constant term in equation (2.15), the limit n->1 is examined. If n is small then $\Delta G(n)$ will be small. Then from equation (2.11) it can be seen that the backward rate b_{n+1} approaches the forward rate f_n, in other words the steady state number density $\rho_{ss}(n)$ for small n approaches the equilibrium value $\rho_{equ}(n)$ (in equilibrium $b_{n+1}=f_n$). So in the limit n->1 $\rho_{ss}(n)/\rho_{equ}(n)$ approaches unity and the constant term equals unity. The other limit is n->∞. For this limit the equilibrium distribution $\rho_{equ}(n)$ goes to infinity which is non-physical. Since the value $\rho_{ss}(n)$ (describing the real distribution of clusters) should have a physical meaning, it must be limited and so the limit of $\rho_{ss}(n)/\rho_{equ}(n)$ as n->∞ equals zero. Thus $J_{ss}(n)$ is given by

$$J_{ss}(n) = \left[\int_1^\infty \frac{dn}{f_n \rho_{equ}(n)}\right]^{-1} . \tag{2.16}$$

Inserting (2.16) in (2.15) now yields

$$\frac{\rho_{ss}(n)}{\rho_{equ}(n)} = J_{ss}(n)\int_n^\infty \frac{dn}{f_n \rho_{equ}(n)} . \tag{2.17}$$

The value of $\rho_{equ}(n)$ is mostly determined by the exponent $\Delta G(n)/k_BT$. Since $\Delta G(n)$ has a maximum the exponential factor will be mostly determined by its value around this maximum. So (2.17) can be simplified using the Laplace or steepest descent method [ABR74],

$$J_{ss}(n) = Z f_{n^*} \rho_1 e^{-\Delta G(n^*)/k_BT} = J(0) e^{-\Delta G(n^*)/k_BT} ,$$
$$Z = \sqrt{\frac{1}{2\pi}\left(-\frac{\partial^2}{\partial n^2}\left[\frac{\Delta G(n)}{k_BT}\right]\right)_{n=n^*}} . \tag{2.18}$$

Again Z is the Zeldovich factor and can be seen as a correction for the non-equilibrium state. With (2.18) the value of J(0) is known and related to $\Delta G(n)$.

The kinetic theory, described so far, forms the basis of the *Classical Nucleation Theory* as described by Becker & Döring [BEC35] and improved by Zeldovich [ZEL43]. It is still among the most well known and widely used theories to describe the process of nucleation. The CNT is based on the so called *capillarity approximation*, that is, the microscopic droplets (of typical size ~100 molecules) are described using the macroscopic properties of the bulk liquid. For example: the surface tension of a critical cluster is assumed to be equal to the surface tension of an infinite liquid plane. Under this assumption, $\Delta G(n)$ is given by [ABR74]

$$\Delta G(n) = -n \cdot k_B T \cdot \ln(S) + \left(\frac{9 v_{molec}^{\,2}}{4\pi}\right)^{1/3} \cdot \gamma \cdot n^{2/3} \qquad (2.19)$$

where v_{molec} is the molecular volume (the liquid molar volume divided by the number of molecules per mol) and γ is the macroscopic surface tension of a liquid plane. Using (2.19) and (2.3) the expression for the critical cluster size yields

$$n^* = \frac{32\pi\gamma^3 v_{molec}^{\,2}}{3 k_B^{\,3} T^3 \ln^3 S}, \qquad (2.20)$$

and the corresponding $\Delta G(n^*)$ yields

$$\Delta G(n^*) = \frac{4\pi\gamma}{3} \cdot \left[\frac{3 v_{molec} n^*}{4\pi}\right]^{2/3}. \qquad (2.21)$$

Inserting (2.20) and (2.21) into (2.19) and using the result in the cluster distribution function as described by (2.1) yields the number of critical clusters.

The nucleation rate, as described in (2.4), can be split into two separate factors. The dominant exponential factor containing $\Delta G(n)^*$ and a kinetic prefactor J(0), the latter one given by (2.18). Following the approach of Becker, Döring and Zeldovich, J(0) is expressed as

$$J(0) = \theta C_n \cdot Zn_1 \,. \tag{2.22}$$

Here n_1 is again the number of monomers and $\theta=1$ the mass accommodation coefficient. C_n^* denotes the number of collisions per unit of time. For a vapor complying to the ideal equation of state, the well known gaskinetic formula can be used,

$$C_{n^*} = \frac{p_v}{(2m_1 \pi k_B T)^{1/2}} \cdot 4\pi \left(\frac{3n^* v_{molec}}{4\pi} \right)^{2/3} . \tag{2.23}$$

Here p_v denotes the partial vapor pressure and m_1 denotes the mass of a vapor molecule. The Zeldovich factor can be derived using equation (2.18) in combination with (2.19) to (2.23). For an ideal gas this yields

$$Z = \sqrt{\frac{\gamma}{k_B T}} \cdot \frac{m_1}{2\pi \rho_{liq}} \cdot \left(\frac{3n^* v_{molec}}{4\pi} \right)^{-2/3} , \tag{2.24}$$

where ρ_{liq} denotes the liquid mass density. The nucleation rate J(n) can now be found by applying (2.4) in combination with (2.19) and (2.22), resulting in

$$\begin{aligned} J(n) &= \sqrt{\frac{2\gamma m_1}{\pi}} \cdot \frac{\theta p_v n_1}{\rho_{liq} k_B T} \cdot e^{-\Delta G(n^*)/k_B T} , \\ \Delta G(n^*) &= \frac{4\pi\gamma}{3} \cdot \left[\frac{3 v_{molec} n^*}{4\pi} \right]^{2/3} = \frac{4\pi}{3} \gamma [r^*]^2 . \end{aligned} \tag{2.25}$$

2.4 A semi-phenomenological nucleation theory

The nucleation rate is a non-equilibrium quantity that is determined by the kinetics of the cluster formation (described in terms of a backward- and forward rate). In the CNT, this was done by relating the coefficient of the backward rate b_{n+1} to the equilibrium number density. This number density turned out to be not valid at critical cluster sizes (it tends to non-physical values for large cluster sizes). In 1977 Katz [KAT77] proposed a different model

for determining b_{n+1} by assuming that the rate at which a cluster evaporates, given by b_{n+1}, is independent of the vapor pressure p_v. Under this assumption, b_{n+1} in the non-equilibrium supersaturated state is equal to its value in a saturated state, which means that ρ_{equ} used in equation (2.10) is now a real equilibrium number density. Using this, J(n) (=J_{ss}(n)) can be written as [KAL95]

$$J(n) = \left[\int_0^\infty \frac{1}{\nu s_n \rho_{n,sat} S^n} dn \right]^{-1} = \left[\int_0^\infty e^{-H(n)} dn \right]^{-1} . \qquad (2.26)$$

Here the function H(n) in the right hand side of equation (2.26) is simply the logarithm of the integrant on the left hand side (note that the function H(n) plays the role of $\Delta G(n)/k_B T$). The function H(n) contains a maximum at $n=n^*$. This value is now considered the critical cluster size. Using this, the exponent can be expanded into a Taylor series around $n=n^*$. Equation (2.26) can now be rewritten (equivalent to the CNT) using the steepest descent method [KAL95]:

$$J(n) = \sqrt{\frac{H''(n^*)}{2\pi}} \nu s_{n^*} S^{n^*} \rho_{sat}(n^*) . \qquad (2.27)$$

The number density at the saturation point $\rho_{sat}(n)$ can be expressed as

$$\rho_{sat}(n) = \rho_1 e^{-\Delta \Omega_{sat}(n)/k_B T} , \qquad (2.28)$$

where $\Delta\Omega_{sat}(n)$ is the grand potential of a n-cluster under the condition that there is no intercluster interaction, which can be found using statistical mechanics. The result yields the so called Fisher theory [Appendix D]. At saturation point it is given by

$$\frac{\Omega_{sat}}{k_B T} = \frac{1}{k_B T} \left[\gamma_{micro} s_1 n^{2/3} + \tau \ln n - \ln(q_0 V) \right] , \qquad (2.29)$$

where γ_{micro} can be expressed in terms of a macroscopic surface tension γ and the, so called, *Tolman length* α_γ. (Tolmans result for the surface tension of curved surfaces). This result can be rewritten yielding [KAL95]:

$$\gamma_{micro}(n) = \gamma\left[1 + \alpha_\gamma n^{-1/3}\right]. \tag{2.30}$$

Using (2.29) and (2.30) it is possible to derive an expression for the number density of n-clusters $\rho(n)$.

$$\rho_{sat}(n) = q_0 e^{-\theta_0(1 + \alpha_\gamma n^{-1/3})n^{2/3} - \tau \ln n} \tag{2.31}$$

where $\theta_0 = \gamma s_1/k_B T$ is a dimensionless macroscopic surface tension. Using (2.31) in combination with the virial equation of state at the saturation point, α_γ can be determined.

$$\alpha_\gamma = -\frac{1}{\theta_0}\ln\left[\frac{p_{sat}}{q_0 k_B T}\right] - 1 + \frac{1}{\theta_0}\ln\left[1 + 2^{-\tau} e^{-\theta_0(2^{2/3} - 1)}\right] \tag{2.32}$$

and with α_γ known, J(n) can be found [KAL95]

$$J(n) = \frac{1}{3}\sqrt{\frac{\theta_0}{\pi}\left(1 + \alpha_\gamma [n^*]^{-1/3}\right) + \frac{9}{2\pi}(\tau - 2/3)[n^*]^{-2/3}} \cdot \frac{p_v s_1}{(2\pi m_1 k_B T)^{1/2}} q_0 S^{n^*} e^{-\theta_0(1 + \alpha_\gamma [n^*]^{-1/3})[n^*]^{2/3} - \tau \ln n^*} \tag{2.33}$$

where the critical cluster size n^* is the real root of the cubic equation (2.34).

$$-n^* \ln S + \frac{2}{3}\theta_0 [n^*]^{2/3} + \frac{1}{3}\theta_0 \alpha_\gamma [n^*]^{1/3} + \tau - \frac{2}{3} = 0 \tag{2.34}$$

In figure 5 (below) the nucleation rates predicted by the classical nucleation theory and the semi-phenomenological theory are given for a water vapor at a temperature of 245 K. From this figure it can be seen that small changes in S can change J(n) for several orders of magnitude.

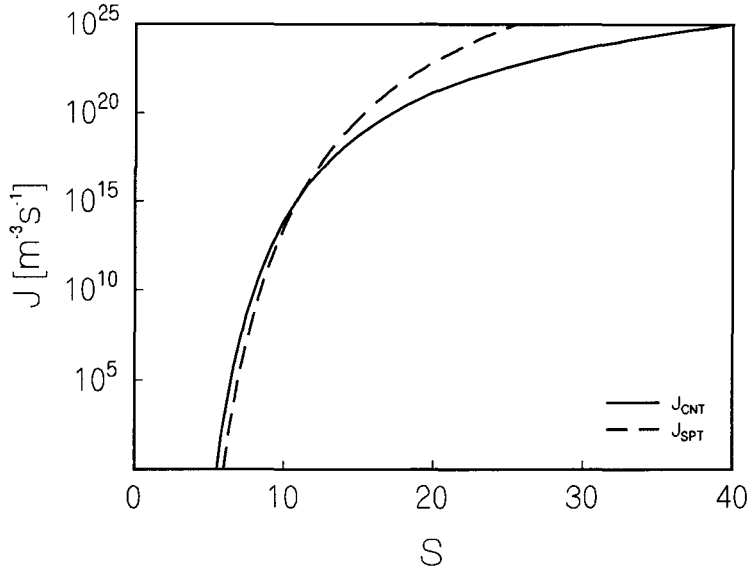

Figure 5 : Plot of J(n) versus S for water vapor at a temperature T = 245 K using the classical nucleation theory (CNT) and the semi-phenomenological theory (SPT).

2.5 Droplet growth

After a droplet is formed it will start to grow, which means mass will condensate on the surface of the droplet. From the kinetics of droplet formation it is known that the steady state solution of the nucleation rate $J_{ss}(n)$ is the sum of two contributions. A diffusion term in the space of cluster sizes (coefficient B in the Fokker-Planck equation) and a drift term (coefficient A in the Fokker-Planck equation). For large clusters, this drift term will become equal to the droplet growth model. For small clusters, however, the contribution of the diffusion term B will be more important. The Fokker-Planck equation (2.12) is now rewritten to

$$1 = -\frac{B}{J_{ss}(n)}\frac{\partial \rho}{\partial n} + \frac{A}{J_{ss}(n)}\rho = \frac{J_{\alpha}}{J_{ss}(n)} + \frac{J_{\beta}}{J_{ss}(n)} \qquad (2.35)$$

and both contributions $J_{\alpha}/J_{ss}(n)$ and $J_{\beta}/J_{ss}(n)$ are plotted against the cluster size n, yielding figure 6. From this figure it can be seen that for small clusters the kinetic process is by far the most important process. For droplets larger then size $n_0 \approx 2n^*$ (yielding a droplet radius larger then $r_0 \approx \sqrt[3]{2}\, r^*$) the macroscopic growth model yields the major contribution to the growth rate ($J_{\alpha} \approx 0$).

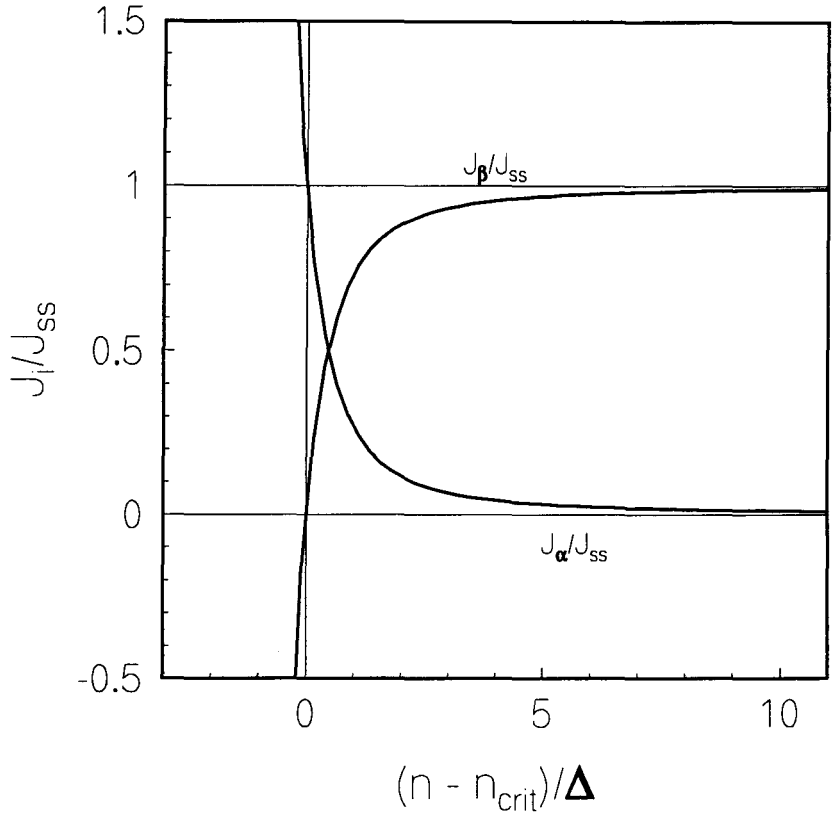

Figure 6 : The contributions $J_\alpha/J_{ss}(n)$ and $J_\beta/J_{ss}(n)$ to the droplet growth rate.

This is an important result, since it gives a good physical description of the lowerbound of the droplet size, for which a macroscopic growth model can be used.

The Gyarmathy droplet growth model, presented below, is an example of a macroscopic growth model. It describes the growth of a droplet as an equilibrium between the amount of mass condensing on the surface of the droplet and the amount of heat the droplet can transfer to its environment. This model assumes that the carrier gas in a gas/vapor mixture is *inert*, meaning that it does not condensate (note that the only contribution of the carrier gas to the condensation process is the absorption of latent heat released during the process of condensation). Assuming the droplets are spherical and that the flow of heat to the interior of the droplet can be neglected. Furthermore it is also assumed that the equilibrium between mass flow and heat transfer is reached instantaneous (the so called *wet bulb approximation*).

The growth of a droplet can be expressed in terms of the mass flux M to the droplet and the energy flux H from the droplet [GYA82]. The result is the

so called *wet bulb equation*,

$$H = M \cdot L \tag{2.36}$$

where L is the latent heat. Hereby it is assumed that there is no energy transfer to the interior of the droplet. The fluxes from and to the droplet can be expressed as

$$H = -2\pi r \lambda Nu_H (T - T_{part}) \tag{2.37}$$

and

$$M = 2\pi r D_M Nu_M (p_v - p_{v,part}) \tag{2.38}$$

where λ is the coefficient of heat conduction for the gas/vapor mixture, T the temperature of the gas/vapor mixture, T_{part} the temperature of the droplet and D_M is a averaged diffusion coefficient given by

$$D_M = \left(1 + \frac{y_g}{y_v}\frac{M_v}{M_g}\right)\bar{M} D \left[V_m (p - p_v)\right]^{-1} . \tag{2.39}$$

Here D is the diffusion coefficient of the gas/vapor mixture, Nu_H and Nu_M are the Nusselt numbers for heat- and mass transport, y_g and y_v are the molar fractions of the gas and the vapor, M_v and M_g are the molar masses of the gas and the vapor, $\bar{M}$ the average molar mass and V_m the average molar volume of the gas/vapor mixture. The total pressure is denoted by p, the partial vapor pressure is by p_v, and the vapor pressure above the curved surface of the droplet by $p_{v,part}$. The latter one can be found from the saturation pressure $p_{v,sat}$ and the droplet radius r using the Kelvin equation [ABR74]

$$p_{v,part} = p_{v,sat}(T_{part}) e^{2\gamma V_{m,liq}/RT_{part}r} . \tag{2.40}$$

Using equation (2.36) in combination with (2.37) and (2.38) it is now possible to write down an implicit equation for the droplet temperature T_{part},

$$\lambda Nu_H (T - T_{part}) = -D_M L Nu_H (p_v - p_{v,part}) \tag{2.41}$$

since the increase in mass is related to an increase in volume and thus an increase in radius, the growth rate can be derived from the above equations (assuming the liquid density is constant)

$$\frac{dr^2}{dt} = \frac{-\lambda Nu_H (T - T_{part})}{\rho_{liq} L} . \tag{2.42}$$

2.6 Effect of carrier gas pressure: Pointing effect

The theories of nucleation presented so far, are so called *single component nucleation theories*. This means that they are based on a vapor component only, in constrast to experiments where a mixture of a carrier gas and a vapor is used. Until now, it was assumed that the carrier gas does not take part in the process of condensation. However, it turns out that the carrier gas pressure can affect liquid-vapor equilibrium.

To find out the effect of pressure on the saturated vapor pressure, the chemical potential of a saturated vapor and a liquid in equilibrium is examined in more detail[2].

$$\mu^o_v = \mu^o_{v,ref} + k_B T \ln\left[\frac{p_{v,sat}(p,T)}{p_{v,sat}(0,T)}\right] \tag{2.43}$$

$$\mu^o_{liq} = \mu^o_{liq,ref} + (p - p_{v,sat}(0,T)) v_{molec} .$$

In (2.43) μ^o is the chemical potential for the pure vapor component, p is the pressure and T the temperature. In equilibrium the chemical potential of the pure vapor μ^o_v and the pure liquid μ^o_{liq} is equal. From this, an expression for the saturated vapor pressure can be derived:

$$\begin{aligned} p_{v,sat}(p,T) &= p_{v,sat}(0,T) e^{(p - p_{v,sat}(p,T)) v_{molec}/k_B T} \\ &\approx p_{v,sat}(0,T) e^{p v_{molec}/k_B T} . \end{aligned} \tag{2.44}$$

[2] The vapor pressure was chosen since it yields the largest effect on the saturation ratio S and thus the nucleation rate J.

where the approximation can be found by neglecting the saturated vapor pressure (which is small compared to the carrier gas pressure). Equation (2.44) describes the so called *Pointing effect*. From this equation it is obvious that if the pressure increases, the saturated vapor pressure decreases. This will affect the saturation ratio and thus the nucleation rate. Also, it can be seen that the Pointing effect depends on the molecular size. For water vapor the effect will be less then for hydrogen-carbon vapors. Nevertheless, from figure 5 it can be seen that even small changes in $p_{v,sat}$ (and thus S) significantly can change the nucleation rate.

HOMOGENEOUS CONDENSATION IN A CONTINUOUS ADIABATIC EXPANSION: NUMERICAL SIMULATION

3.1 Introduction

The theory of nucleation as described in chapter 2 can be examined using a numerical simulation. In this simulation, an amount of gas/vapor is subjected to an adiabatic pressure fall. For the remainder of the chapter, the volume containing the gas/vapor is referred to as the *system*. It is assumed that the system is isolated in a sense that it conserves both matter and energy. This system responds to the adiabatically pressure fall by changing the volume accordingly. The known *initial conditions* are the initial pressure p_0, the initial temperature T_0 and the initial partial vapor pressure $p_{v,0}$. Furthermore the pressure is a known function of time, or an *input parameter*. The desired *output parameters* are the extinction coefficients for light of two wavelengths. These quantities are of interest since they can be measured (see chapter 4).

3.2 Derivation of the basic equations

The experiment can be described using three conservation laws. They are conservation of mass, momentum and energy. Of these three equations, conservation of momentum, can be discarded, since solving this equation yields the pressure signal which is an input parameter. The remaining two conservation laws are given by

$$\frac{d\rho V}{dt} = 0 , \tag{3.1}$$

$$\rho \frac{de}{dt} + p\rho \frac{d1/\rho}{dt} = 0 . \tag{3.2}$$

Here e denotes the specific entropy of the gas/vapor mixture and ρ the density of the gas/vapor mixture. If the carrier gas is ideal, that is, it does not take part in the condensation process, then the conservation of mass can be separated into two independent equations

$$\frac{d}{dt}\left[\rho_{gas} V\right] = 0 , \tag{3.3}$$

with ρ_{gas} the density of the carrier gas and

$$\frac{d}{dt}\left[\rho_{v} V + \rho_{liq} V\right] = 0 , \tag{3.4}$$

were ρ_v is the vapor density and ρ_{liq} the liquid density. For the process of condensation only equation (3.4) is of importance. It describes the physical background of a process that is referred to as *vapor depletion*: if the amount of liquid increases, then the amount of vapor has to decrease.

The amount of liquid formed is dependent on the number of droplets formed and the growth of the existing droplets. Nucleation (formation of droplets) and droplet growth have been covered extensively in the previous chapter. For now it is enough to assume that there is a general nucleation model describing the nucleation rate J and a general growth model describing the growth rate dr/dt of a droplet with radius r. The liquid mass m_{liq} formed per unit of time can now be expressed in terms of the nucleation rate and the growth rate, yielding

$$\frac{dm_{liq}}{dt} = \frac{d}{dt}\left[\rho_{liq} V\right] = J(t) V(t) \rho_L \frac{4}{3} \pi r_0^3(t) + \int_0^t J(\xi) V(\xi) \rho_L 4 \pi r^2(t,\xi) \frac{dr(t,\xi)}{d\xi} d\xi . \tag{3.5}$$

Here ρ_{liq} is the density of the liquid mass in the system and ρ_L is the density of the liquid in a droplet (which is assumed to be constant). The first term on the right hand side describes the increase in the liquid mass due to the formation of J·V droplets having a radius $r_0(t) \approx \sqrt[3]{2}\, r^*(t)$. The second term describes the increase in liquid mass due to the growth of all droplets already existing in the system. The notation $r(t,\xi)$ denotes the radius of a droplet at current time t formed at an earlier time ξ. It can be computed using

$$r(t,\xi) = r_0(\xi) + \int_{\xi}^{t} \frac{dr(\tau,\xi)}{d\tau} d\tau \qquad (3.6)$$

If vapor condenses and forms liquid, an amount of latent heat is released. This latent heat can be seen as a energy source inside the system. If there is no homogeneous condensation and if the vapor is considered ideal then the solution of energy conservation (in combination with mass conservation) will yield the isentropic gas relations. However, if droplets are formed then the conservation of energy will gain an extra term,

$$\frac{dh}{dt} + L\frac{d}{dt}\left[\frac{m_{liq}}{\rho V}\right] = \frac{1}{\rho}\frac{dp}{dt} . \qquad (3.7)$$

Here (3.2) has been rewritten in terms of the specific enthalpy h. The isentropic solution of the energy conservation equation (3.7) can be found by solving (3.1) and (3.7) with m_{liq} set to zero.

Unlike the mass conservation law, the energy conservation law cannot be split in one equation describing energy conservation the carrier gas and one equation describing energy conservation of the vapor. The reason is that if energy is added to the system it will be homogeneously spread over the entire system.

After the solution of (3.4), (3.5), (3.6) and (3.7) is found, it must be presented into a form so that it can be compared with experimental result. The detection method (described in more detail in chapter 4) is based on the extinction of light emitted by a laser. This extinction can be theoretically computed using the Mie theory [KER69] (the Mie-theory describes the scattering of light at spherical particles by solving the Maxwell equations).

If light of a given wavelength λ and intensity I_0 illuminates a number of droplets, the intensity I of the transmitted light will be less than I_0. This is caused by absorption and scattering of the inciting light. The relation between the illuminating intensity I_0, the transmitted intensity I and the *extinction coefficient* β is given by the Lambert-Beer law

$$\frac{I}{I_0} = e^{-\beta L} , \qquad (3.8)$$

where L is the length of the optical path and β is the extinction coefficient which emerges from the Mie-theory.

The extinction coefficient for a spherical droplet of radius r depends on the wavelength λ of the incited light and the index of refraction m of the droplets. Introducing a size parameter $\alpha=2\pi r/\lambda$, it can be expressed in terms of the extinction efficiency Q_{ext}, also emerging from the Mie theory [KER69]

$$\beta(r,\lambda) = \pi r^2 Q_{ext}(\alpha,m) . \tag{3.9}$$

For a cloud of droplets with a size distribution f(r), the total extinction can be found by summing the individual contributions of the droplets. The result is given by

$$\beta = \int_0^\infty f(r)\pi r^2 Q_{ext}(\alpha,m)dr . \tag{3.10}$$

Since the droplet size distribution function is related to the nucleation rate and the growth model, the extinction coefficient as a function of time now becomes directly related to the nucleation rate J and the droplet growth rate dr/dt.

$$\beta(t) = \int_0^\infty J(\xi)\frac{V(\xi)}{V(t)}\cdot\pi r^2(t,\xi)Q_{ext}(r(t,\xi),m)d\xi \tag{3.11}$$

3.3 Numerical simulation: method of solution

Equations (3.4), (3.5), (3.6) and (3.7) form a complete system of equations that can be solved if the initial conditions are known. The method used is called *Euler explicit*, which means that the solution at time t_{n+1} is based on the solution at time t_n. The flowchart of an iteration during the simulation is shown in figure 5. In the discussion of the iteration, the result of the previous iteration or *old state* is labeled 'n', while the result of the current iteration or *new state* is labeled 'n+1'.

The iteration starts with a known solution of the previous time step and the new pressure p_{n+1}. Using p_{n+1} and the old thermodynamic state (p_n,T_n), the

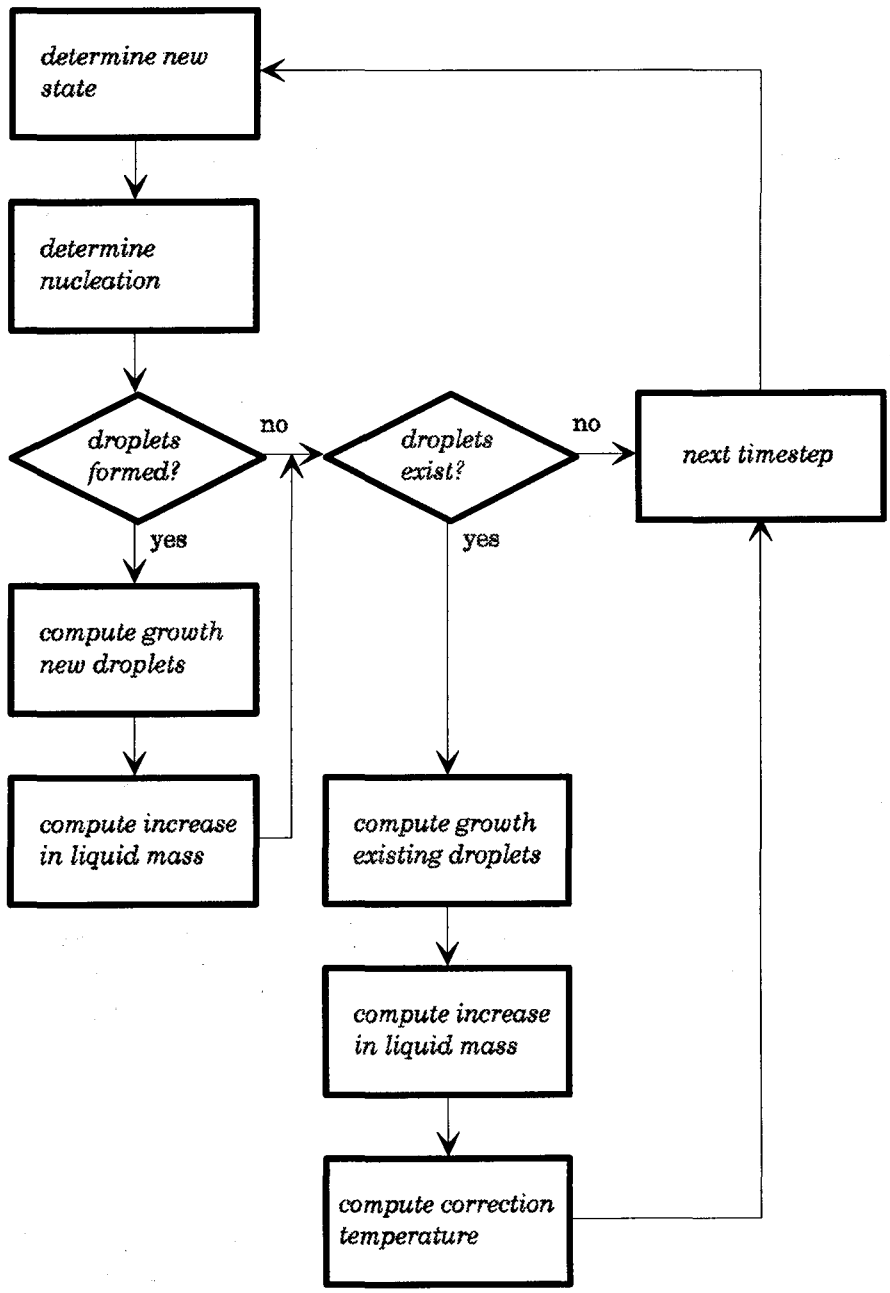

Figure 7 : Flowchart of a single iteration in the numerical simulation of the homogeneous condensation process.

new thermodynamic state of the system (p_{n+1},T_{n+1}) is computed based on an isentropic expansion and an equation of state. After this, the thermodynamic state is kept constant for the duration of the time interval $\Delta t = (t_{n+1} - t_n)$.

The nucleation rate is now determined based on the new thermodynamic state. If the nucleation rate is large enough to form droplets then these droplets are allowed to grow during half a time step Δt using an initial radius or r_0 (see chapter 2). This is allowed because the steady state solution of the nucleation rate is reached in a time $\tau_{ss} \ll \Delta t$. Since droplets are formed continuously during the entire time interval Δt, the new formed droplets have an average time $\Delta t/2$ to grow (note that the nucleation rate is constant during the time interval Δt).

Following the nucleation, the growth of all existing droplets is computed, excluding the newly formed droplets. This is a loop ranging from the first droplets formed to the droplets formed at the previous time step. Computing the growth of the existing droplets can only be done if the number density and radius of the droplets are known. These data need to be stored in an array that will grow in size as long the nucleation produces droplets.

Whenever droplets are formed or grow, the amount of mass needed for formation or growth is computed and added to the total mass condensing. At the end of the iteration, the total mass condensing is used to compute the new gas/vapor composition and the amount of latent heat released. This is then used to compute an increase in the current temperature ΔT_{n+1}, after which the next iteration can be entered.

3.4 Numerical simulation : results

As stated in paragraph 3.2, the numerical simulation uses a known pressure function. This can either be a measured signal or function describing the pressure in time. The results presented in the remainder of this chapter are obtained using the following pressure-time relation:

$$p(t) = p_0 \left(0.05 + 0.95 e^{-t/\tau}\right) \qquad (3.12)$$

The description of (3.12) incorporates this characteristic exponential pressure decrease of an adiabatic expansion. The value of τ is the characteristic time of the expansion. It determines the slope of the signal and can be used to alter the speed of the expansion.

In figures 6 and 7 the results of an expansion are shown for a Helium/Water mixture using an initial pressure p_0=5 bar, initial temperature T_0=295 K and initial partial vapor pressure $p_{v,0}$=2000 Pa. In the beginning of

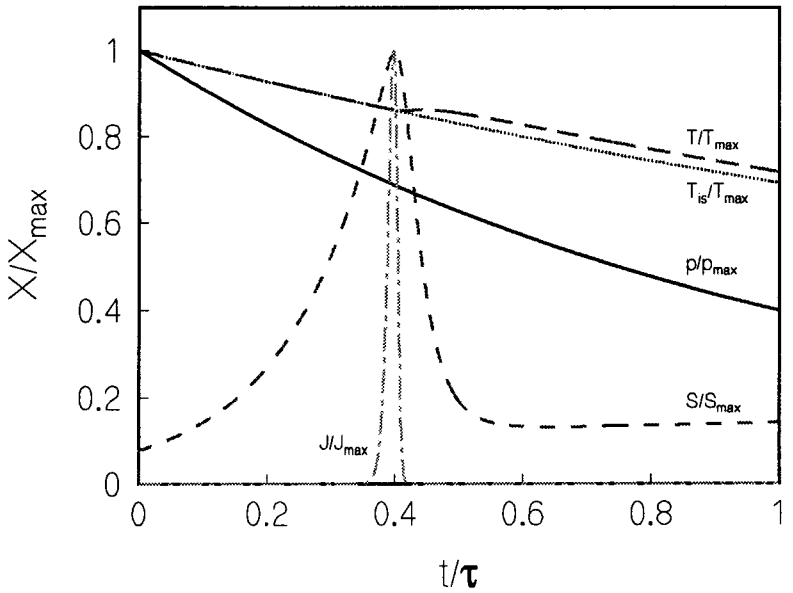

Figure 8 : Simulation showing p, T, T_{is}, J and S using the pressure-time relation (3.12) with τ=20 ms for a Helium / Water mixture with an initial pressure p_0=5 bar, an initial temperature T_0=295 K and an initial vapor pressure $p_{v,0}$=2000 Pa.

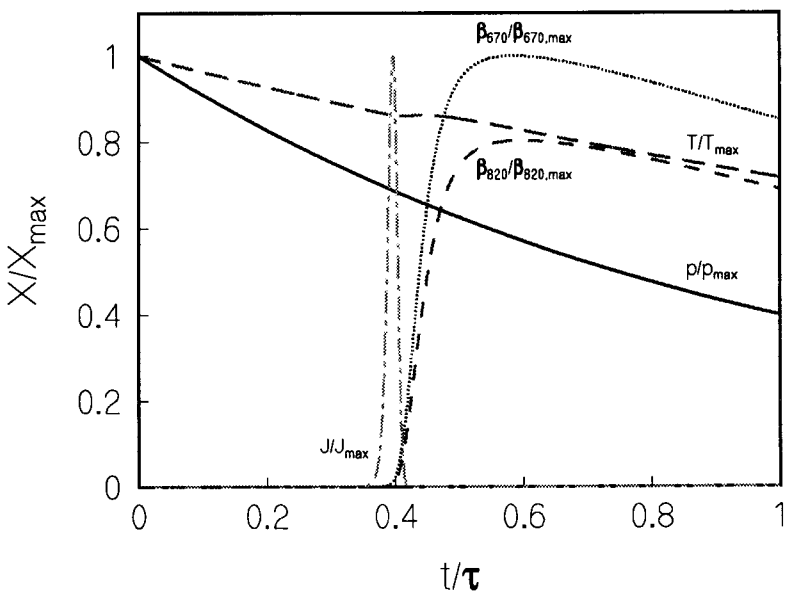

Figure 9 : Simulation showing the extinction coefficients of the 670 nm and 820 nm wavelengths, together with p, T T_{is} and J.

the expansion, no droplets are formed. So the solution of the mass conservation law and the energy conservation law yield the isentropic gas relation. This can be seen from figure 6, where in the beginning of the expansion the solution of T matches the isentropic solution T_{is}.

For constant temperature T the nucleation rate J will be a monotonously increasing function of S (see chapter 2). For constant saturation S, the nucleation rate will be a monotonously increasing function of T. During the expansion the temperature is lowered adiabatically, this will decrease J. On the other hand, a lower temperature will increase S exponentially. This will increase J. Since the latter term greatly exceeds the first term, the net result is an almost exponentially increase in S.

At $t/\tau \approx 0.35$[1] the first droplets are formed. From this point on the expansion will no longer be isentropic. The droplets now entering the expansion will have a double impact on the saturation ratio S. First: due to vapor depletion, the vapor pressure will decrease extra (note that the vapor pressure also decreases due to the expansion). Second: due to the release of latent heat, the temperature T will increase. As a result the rate at which S increases is reduced.

After $t/\tau \approx 0.35$, S will be affected by vapor depletion (and to a lesser extent the latent heat). The saturation ratio S and the nucleation rate J increase. This increase in J will rapidly increase the number of droplets in the system, and the formation and growth of these droplets will eventually reduce the amount of vapor substantially.

The nucleation reaches its maximum at $t/\tau \approx 0.39$. At this point many droplets are already formed and the saturation ratio S no longer increases exponentially (which can be seen by looking at the slope of S near the maximum of the nucleation in figure 6). Only slightly later in time (at $t/\tau \approx 0.40$) the saturation rate also reaches its maximum.

The rapid decrease in vapor density is accompanied by a rapid increase in the release of latent heat in the system. This will affect the temperature, as can be seen from figure 6 where the effect of latent heat is visible as a perturbation in the temperature. For water, the latent heat is large, so if enough vapor is available in the system the increase in temperature can even exceed the adiabatic decrease in temperature due to the expansion.

In figure 7 it can be seen that the extinction signals emerge at approximately the same time the nucleation pulse reaches its maximum. However, this is generally not true. For different gas/vapor mixtures, τ values and/or initial conditions (p_0, T_0 and $p_{v,0}$) the onset of the optical signals can be different. In order to show the difference in extinction between two different wavelengths,

[1] The onset of the nucleation rate depends on the gas/vapor mixture, the value of τ and the initial conditions (p_0, T_0 and $p_{v,0}$) used.

the signal of the 820 nm wavelength in figure 7 is normalized with the maximum of the 670 nm wavelength.

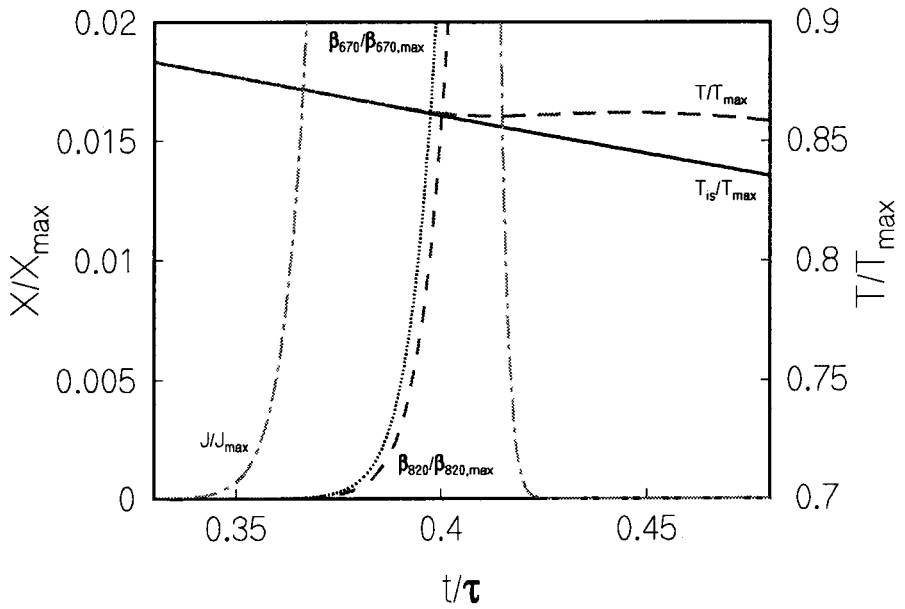

Figure 10 : Detail of the onset of the extinction signals of figure 7

In figure 8 the onset of the extinction signals is shown in more detail. Also shown here are the nucleation rate J, the temperature T and the isentropic temperature T_{is}. From this figure it can be seen that the effect of the latent heat only becomes visible at the end of the nucleation pulse. This implies that the droplet growth only becomes important after the nucleation pulse, so the onset and the first increase in the extinction are (for the larger part) caused by nucleation and droplet growth under isentropic conditions only. After the nucleation, the extinction signals of the 670 nm wavelength and the 820 nm wavelength continue to rise. At this stage, no new droplets are formed and the increase in extinction is due to droplet growth only.

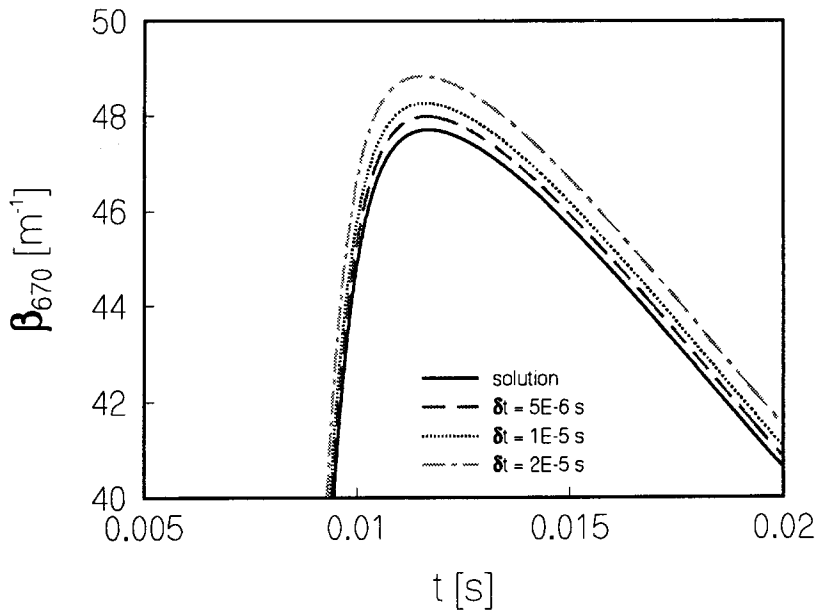

Figure 11 : The effect of a change in time step Δt on the extinction of the 670 nm wavelength.

3.5 Numerical convergence and error analysis

The numerical simulation was tested for convergence. This was done by running a simulation of the experiment in figure 6 for three different time steps Δt. The behavior of β_{670} for these simulations is shown in figure 9 (the behavior of β_{820} yields the same result so it is not shown). From these simulations it can be seen that for a time step $\Delta t=5\cdot10^{-6}$ s the solution is within 1% of its (estimated) limit for Δt=0 s.

In order to improve the solution, the knowledge is used that the Euler explicit method is a first order method, meaning that the solution converges linearly towards the analytical solution. Running the simulation twice, for two different time steps Δt_1 and Δt_2 will yield two solutions $\Sigma_1(t,\Delta t_1)$ and $\Sigma_2(t,\Delta t_2)$. Using linear extrapolation, the analytical solution Σ(t) (Δt=0 s) can be found.

$$\Sigma(t) = \Sigma_1(t,\Delta t_1) - \left(\frac{\Sigma_1(t,\Delta t_1) - \Sigma_2(t,\Delta t_2)}{\Delta t_1 - \Delta t_2} \right) \Delta t_1 . \qquad (3.13)$$

The solution obtained using this method is also shown in figure 9. The verification of this method can be found in Appendix E, where the solution of the simulation for $(\Delta t_1,\Delta t_2) = (1\cdot10^{-5},5\cdot10^{-6})$ s is compared with the solution of

$(\Delta t_1,\Delta t_2) = (2\cdot10^{-5},1\cdot10^{-5})$ s. It can be seen that both pairs $(\Delta t_1,\Delta t_2)$ converge to the same analytical solution.

As stated in the introduction of this chapter, the experiment is simulated using a number of initial conditions: p_0, T_0 and $p_{v,0}$. In the experiments (see chapter 4), these quantities are subjected to errors in measurement. It is assumed that the initial pressure p_0 is known with enough accuracy compared to T_0 and $p_{v,0}$. So only the effects of a ±5% variation on $p_{v,0}$ and a ±1% variation on T_0[2] are analyzed.

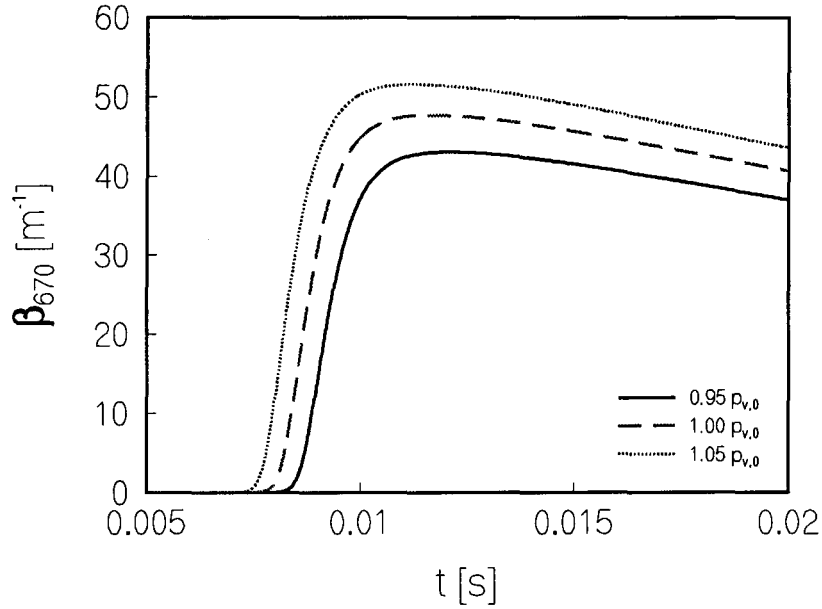

Figure 12 : The effect of a change in vapor pressure on the simulation.

In figure 10, the effect of the ±5% change in vapor pressure on the extinction coefficient β_{670} is shown (the result for the 820 nm wavelength is the same so it is not shown). From this figure it can be seen that an increase in vapor yields an increase in extinction. Also, the onset of the optical signal is shifted to an earlier time.

Assume the saturation rate at a time t' has a value of S', and the corresponding nucleation rate has a value J'. If more vapor is introduced then this value of S' will be reached at an earlier time (figure 6). Since the extinction coefficient is coupled to the nucleation rate, the onset of β will also shift to an earlier time.

[2] In reality the temperature T_0 can be measured with a higher accuracy. The value ±1% is to be considered an upper bound.

The increase in extinction cannot be explained directly by either more droplets or larger droplets. Although more vapor is introduced it is not necessarily so that more droplets are created, since the growth rate is also affected (more vapor will yield a higher saturation and thus a higher growth rate). The droplets formed at the beginning of the nucleation will become larger and thereby again reducing the amount of vapor available for the creation of new droplets. The increase in extinction will most likely be a combination of both effects.

The effect of a ±1 % change in the initial temperature T_0 on β_{670} is shown in figure 11 (the result for β_{820} is the same so it is not shown). From this figure it can be seen that the onset of the extinction shifts to an earlier time with decreasing T_0.

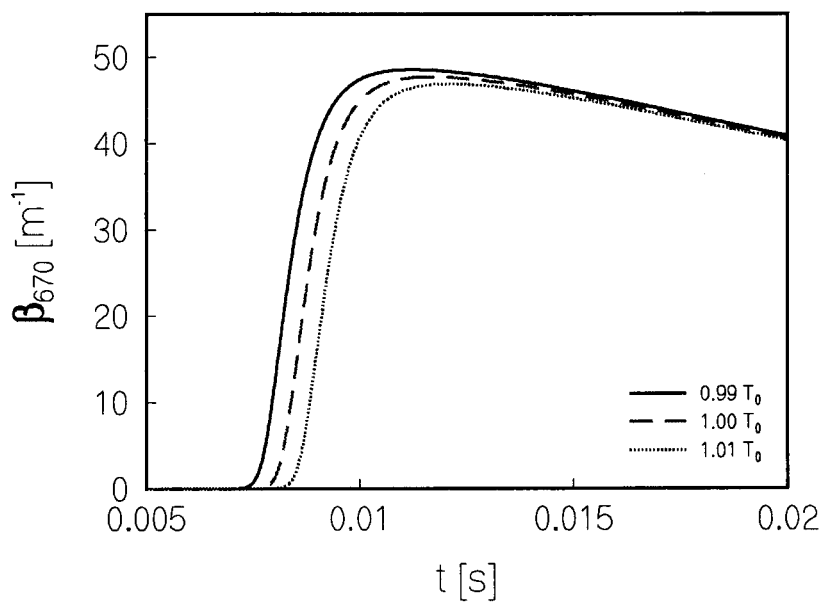

Figure 13 : Effect of a change in initial temperature T_0 on the extinction.

This can be explained using the definition of the saturation ratio S (equation (1.1)). A lower temperature yields an exponentially higher value of the saturation ratio, so the nucleation rate will increase accordingly. Thus the onset will shift to the left. The fact that the droplets are formed at a higher saturation ratio will cause a higher growth rate. This will increase the effect of vapor depletion. The net effect is fewer droplets with larger radius. Apparently the larger radius cannot compensate the effect of fewer droplets (as can be seen from decrease in the maximum of β_{670} in figure 11).

Just like the initial conditions of the experiment, the *process parameters* (e.g. surface tension γ, diffusion coefficient D etc.) are also parameters that are subjected to errors. Most of these parameters are computed using empirical

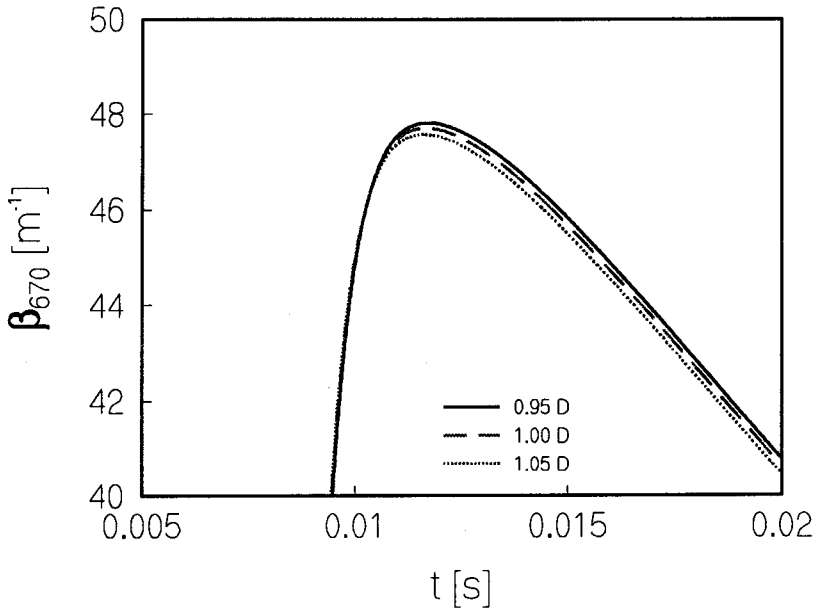

Figure 14 : The effect of a change in the diffusion coefficient on the extinction of the 670 nm wavelength using the expansion of figure 6.

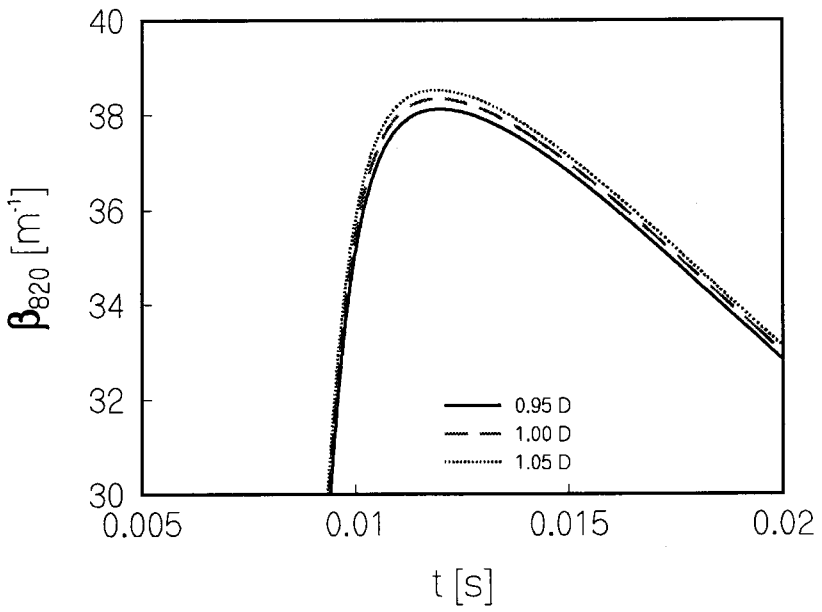

Figure 15 : The effect of a change in the diffusion coefficient on the extinction of the 820 nm wavelength using the expansion of figure 6.

relations, based on measurements found in the literature. These relations always inhibit an uncertainty.

Two process parameters will be discussed: the diffusion coefficient D which is important in the model of Gyarmathy describing the growth rate and the surface tension γ, which is an important parameter in the nucleation models. The first parameter regarded is the diffusion coefficient. The effect of variations on the diffusion coefficient are shown in figures 12 and 13. From these figures it is immediately apparent that the effect of a change in the diffusion coefficient on the extinction β_{670} is opposite to the effect of a change in the diffusion coefficient for the extinction β_{820}. This effect can be explained by looking at the extinction of a droplet as a function of its radius (shown in figure 14) and the number of droplets.

The largest droplets in the experiment have a radius larger then $8 \cdot 10^{-7}$ m. From figure 14, it can be seen that for droplets of this size, the extinction β_{670} ($=\pi r^2 Q_{ext}$) reaches a maximum (for droplets of larger size the extinction β_{670} even decreases, whereas the extinction β_{820} still increases). If the diffusion coefficient is increased, the droplet growth rate will increase and the average droplet size will grow larger. So more droplets will have a radius larger then $8 \cdot 10^{-7}$ m and the net result will be less extinction.

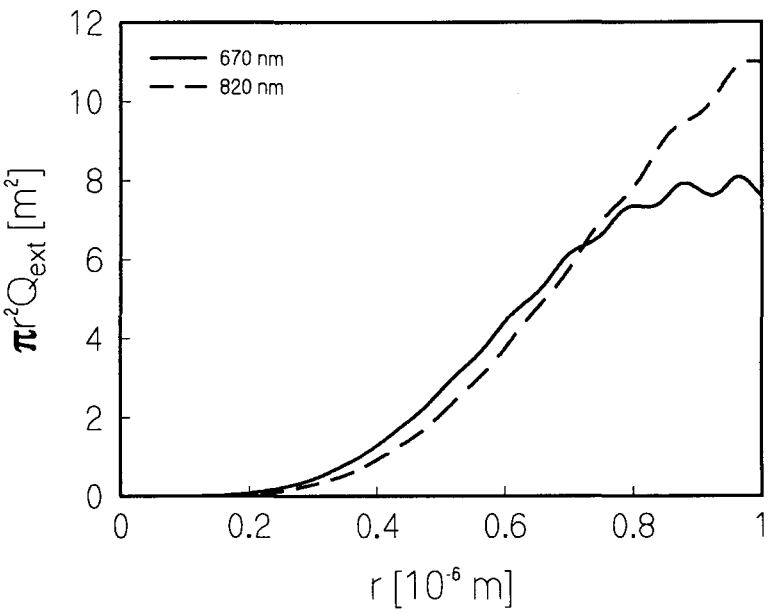

Figure 16 : The extinction of a droplet versus the radius of the droplet for light of 670 nm and 820 nm

The second effect that should be taken into consideration is the number of droplets. Since a larger diffusion coefficient yields a larger growth rate of the droplets, this will also yield less droplets. The result of this can add to the first effect. The reason that the extinction β_{820} still increases (whereas β_{670} decreases) is that the increase in β_{820} can overcompensate the effect of fewer droplets with larger radius.

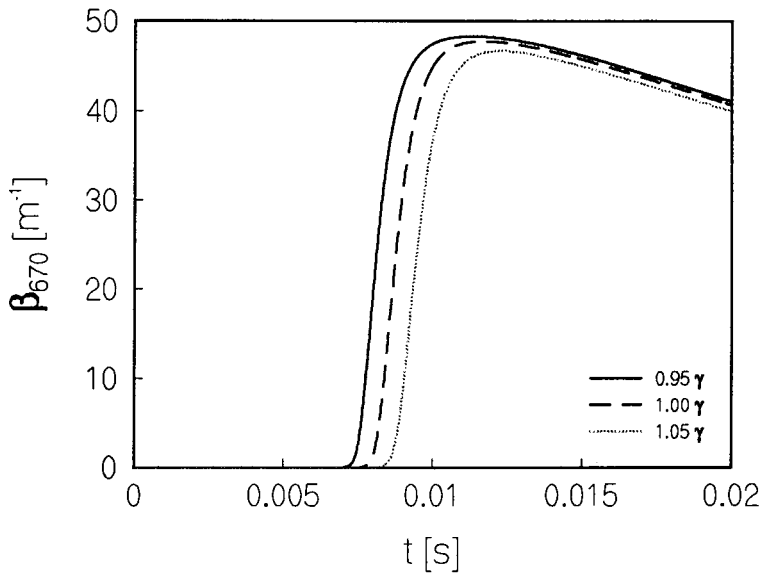

Figure 17 : The effect of a change in surface tension γ on the extinction of the 670 nm wavelength using the expansion of figure 6.

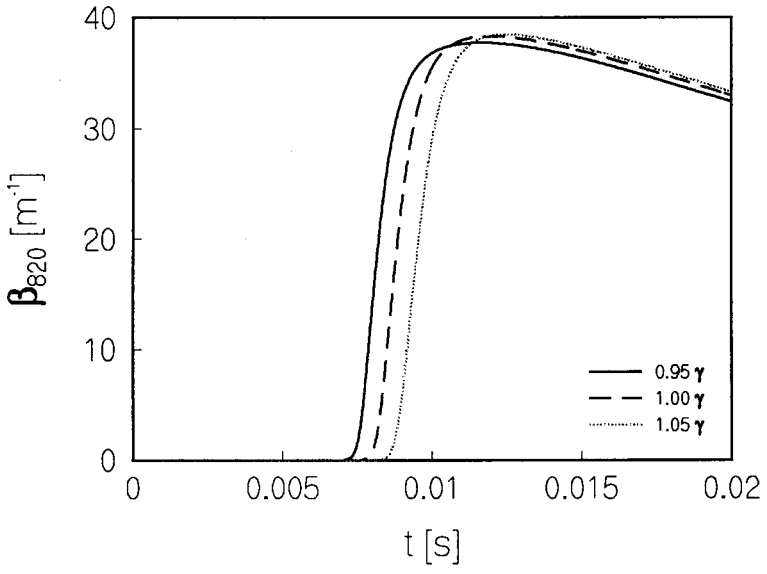

Figure 18 : The effect of a change in surface tension γ on the extinction of the 820 nm wavelength using the expansion of figure 6.

The last parameter examined in this chapter is the surface tension γ. The effect of a change in γ on the extinction coefficients of the 670 nm wavelength and the 820 nm wavelength is shown in figures 15 and 16. From these figures, two effects become visible.

First there is a shift in the onset of the extinction towards a later time. This is caused by an increase in γ which will increase $\Delta G^*(n)$. Nucleation can only then occur if the $\Delta G^*(n)$ is sufficiently small. So if $\Delta G^*(n)$ is increased, a larger value of S is needed to reduce $\Delta G^*(n)$ sufficiently the effect and hence the onset of the nucleation will shift towards a later time.

Again, as with the change in the diffusion coefficient, it can be observed that the maximum of β_{670} decreases with increasing γ and the maximum of β_{820} increases with increasing γ. The explanation for this is the same as with the variation in the diffusion coefficient. Note that again this effect will be a combination of both droplet numbers and droplet sizes.

HOMOGENEOUS CONDENSATION IN A CONTINUOUS ADIABATIC EXPANSION : EXPERIMENTS

4.1 Introduction

As mentioned in the first chapter, the formation of droplets can be studied using several different techniques. In this chapter a description of the expansion cloud chamber is presented. The experimental results also presented were performed using this experimental technique. The results were analyzed using the numerical model of chapter 3. Measurements were done for Helium/Water mixtures

4.2 Experimental setup

The experimental setup, shown in figure 19, consists of an expansion chamber (EV) and a vacuum chamber (VV) separated by a fast opening electro-magnetic valve (M1). The expansion chamber is connected to a circulation section containing a pump (RP). Two valves (MK1 and MK2) allow the expansion chamber to be separated from the circulation section. At the end of the vacuum chamber, a vacuum system is installed, containing an vacuum pump (for low vacuum: ~10 Pa) and a turbo molecular pump (for high vacuum: $\sim 10^{-3}$ Pa). Both pumps are connected with VV by the valve h2.

The expansion chamber contains two sensors. A Druck piezo resistive pressure transducer (type PDCR 200) is used to measure the initial pressure. A Kistler (type 603B) transducer is used to measure the pressure change during the adiabatic expansion. A second Kistler (type 603B) is installed in the tubing between MK1 and the circulation pump RP. This pressure transducer is used to measure the pressure pulses during the mixing of the gas and the vapor. The tubing between MK2 and AB1 contains a capacitive relative humidity gauge (HUMICAP HMP 12, n° 239043). This gauge is used to measure the amount of water vapor in the system. It also measures the temperature of the gas/vapor mixture. The tubing between IK and the circulation pump also contains a pressure transducer (Barocel type 600AB), which can be used to measure the vapor pressure directly. The Barocel can only be used for low pressures (lower than approximately 10^4 Pa).

The preparation of an experiment contains two steps. First, the remaining gas/vapor of previous experiments needs to be removed. This can be done by creating a vacuum in the entire experimental setup. To create a vacuum, first

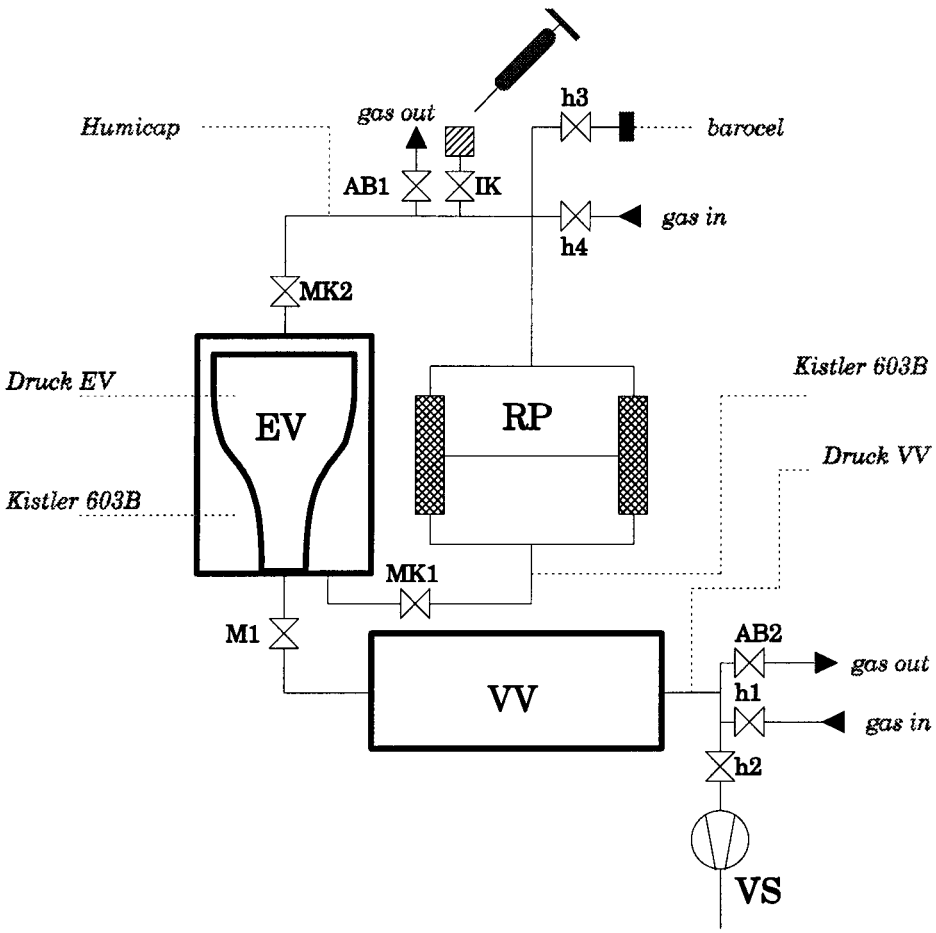

Figure 19 : Schematic diagram of the experimental setup

any redundant gas/vapor is reduced until the pressure in the experimental setup reaches atmospheric pressure. This is done by first opening h_4, followed by AB1. Next the magnetic valve M1 is opened together with AB2. If both sections, EV & RP and VV, are at atmospheric pressure, then the valves MK1 and MK2 can be opened. After this, AB1 and AB2 are closed and the vacuum pump is activated. Then h_2 can be opened.

The system is held at low vacuum for approximately 30 minutes, which is long enough to remove nearly all remnants of previous experiments. After that the valve h_2 is closed and the vacuum pump is deactivated. Now the magnetic valve can be closed for the next step in the preparation of an experiment.

In order to create a gas/vapor mixture, the expansion chamber and the circulation section should form a single contiguous compartment. To create this, all valves should be closed with the exception of MK1 and MK2. Now an injection needle (Hamilton-Bonadu, Schweiz, type1710, capacity 100 µl) is filled with an amount of water (in our case either 30 µl or 10 µl was used). Then the injection valve IK is opened and the liquid is injected into the vacuum.

Immediately after injection, the valve IK is closed and for a short duration,

the mixing pump RP is activated. After the pump is deactivated the valve h_4 is openened. Next the expansion chamber and the circulation section are filled with gas up to approximately 1 bar. Then h_4 is closed and the mixing pump is restarted.

The injection takes place at vacuum, so most liquid will evaporate immediately. However, the magnetic valve used in the experimental setup needs a minimum pressure difference of 0.7 bar between the expansion chamber and the vacuum chamber in order to fully seal of both compartments. This is the reason why, shortly after injection, an amount of gas is let into the expansion chamber and the circulation section. This amount must be large enough to allow the magnetic valve to function properly, but it should be kept as small as possible, since the process of diffusion decreases with increasing pressure and this makes the mixing process less efficient.

The mixing pump remains active until the gas/vapor mixture has reached a homogeneous composition. This was verified using the Humicap[1]. After the pump is deactivated, the valve h_4 is opened and a new portion of gas is let in until the pressure reaches the initial value wanted for the experiment. Now the valve h_4 is closed again and the mixing pump is reactivated. If the gas/vapor mixture has reached a homogeneous composition, the valves MK1 and MK2 are closed. Now the experiment is started by opening the electromagnetic valve M1.

The mixing pump contains 6 strong electro-magnets. When used for a longer period, these electro-magnets heat up. Since they are placed around the tubing, the tubing will also heat up locally (a temperature difference of approximately 1 K was found between the gas in the tubing of the circulation section and the gas in the expansion chamber). The gas/vapor mixture inside the tubing will (in a homogeneous situation) be in equilibrium with the vapor absorbed at the innerwalls of the experimental setup. However, if locally the temperature of the innerwalls is increased then the gas/vapor, near these heated walls, will have a different composition from the gas/vapor mixture elsewhere. This is an inhomogeneous and thus undesired situation. So, the electromagnets cannot be used continuously for a longer period. Instead, the mixing pump is used in short periods of approximately 5 minutes.

For the Druck transducers two calibrations were created (Appendix C). For low pressures (up to ~20 bar) a calibrated Wallace & Tiernan pressure sensor was used as a reference (accuracy: ±0.025 bar). For high pressures (20 ~ 100 bar), a Druck Digital Pressure Indicator (DPI, type 601, accuracy: ±0.2 bar) was used as a reference. The high pressure calibration is accurate up to 0.2% full scale (±0.2 bar) the low pressure calibration is accurate up to 0.4% full scale (±0.08 bar).

For the Kistler both the method of calibration and the results are also

---

[1] The output of the Humicap was recorded using an xt-writer. For a homogeneous gas/vapor mixture the xt-writer showed a horizontal line.

described in Appendix C. The experimental results were obtained using the high pressure calibration. The accuracy of this calibration is 0.2% full scale.

The experimental setup showed a leakage rate of 0.5 bar/hour in the pressure range 60 to 80 bars. In the range 40 to 60 bar the leakage rate dropped to approximately 1.0 bar/hour. For pressures lower then 40 bars, no significant leakage rate was measured (within the approximately 3 hrs time needed to prepare an experiment).

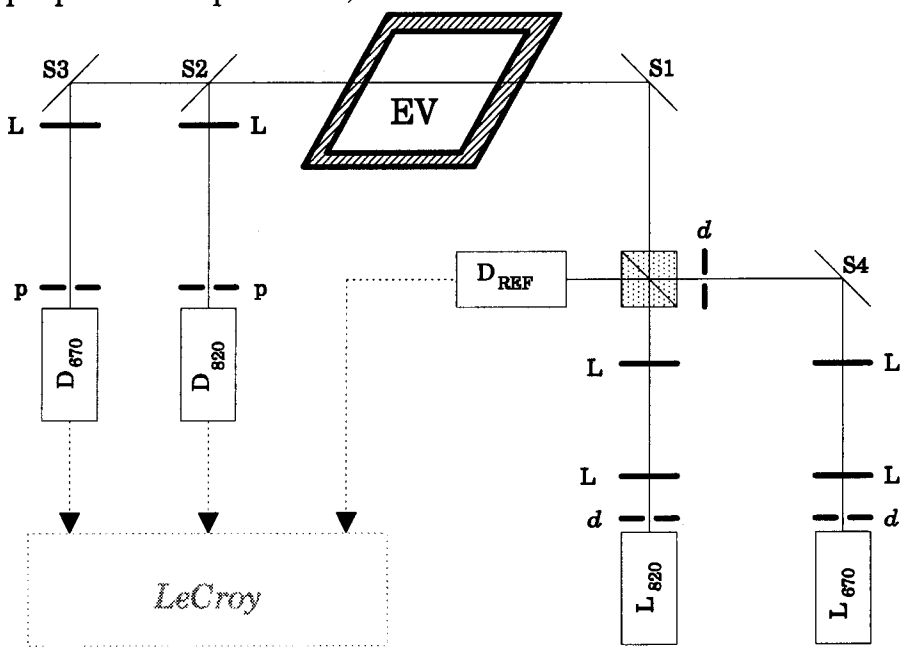

Figure 20 : The optical setup used to measure extinction.

In figure 20 the optical setup is shown, used to measure the extinction of light of two wavelengths. It contains two solid state lasers, some optical tools to direct the light from these lasers through the windows in the expansion chamber EV (constructed using BK7) and detectors, to measure the amount of light transmitted.

One laser has a wavelength of 670 nm (labeled L_{670}) and is referred to as the *red laser*. The other laser has a wavelength of 820 nm (labeled L_{820}) and referred to as the *infrared laser*. Both laser beams first pass a diaphragm *d*, used to decrease the initial intensity of the laser beam. After that, both beams pass an optical system containing a positive lens with a focus of 50 mm followed by a positive lens with a focus of 15 mm (the lenses are labeled L). The distance between both lenses is 65 mm. The two pair of lenses are used to decrease the diameter of the laser beams to approximately 1 mm.

The infrared laser beam is now directed at the mirror S1. From there it is redirected towards the windows in the expansion chamber. In between the pair of lenses and the mirror S1 a cubic beamsplitter is positioned. The infrared laser beam passes over this beamsplitter.

The red laser beam is directed via the mirror S4 on the beamsplitter. A second diafragma *d* is placed before the beamsplitter to collect the fringes round the red laser beam.[2].

The beamsplitter separates the incoming red laser beam into two beams. One laser beam passes undeflected through the beamsplitter and illuminates a diode labeled D_{REF}. This diode is used as a reference to measure the changes in the intensity of the red laser beam. The second red laser beam will be deflected for 90° and incites on the mirror S1. From there it is redirected towards the windows in the expansion chamber.

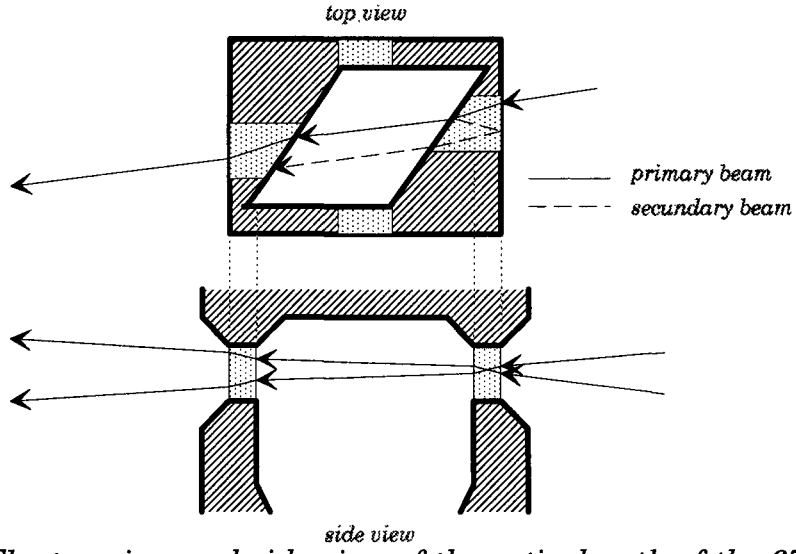

Figure 21 : The top view and side view of the optical path of the 670 nm laser beam and the 820 nm laser beam as they travel through the expansion chamber.

The optical path of the red and the infrared laser beam is shown in figure 21, which shows in more detail what happens when the two laser beams enter the expansion chamber EV. From this figure it can be seen that the windows used are not opposite to each other. This allows the incoming laser beam to be directed at a larger angle which is necessary to separate the primary laser beam and the secondary laser beam (created by reflection at the inside of the window), thus preventing interference.

After passing the expansion chamber, the infrared laser beam (figure 39) incites on the mirror S2 (which is positioned low enough below the red laser beam). From there it is redirected to a positive lens L. In the focus point of the lens, a diode (labeled D_{820}) is placed that collects the light of the infrared laser beam transmitted by the expansion chamber. Slightly before the diode a pinhole

[2] It was observed that the red laser produced a beam containing an interferention pattern.

is placed to intercept scattered light[3].

The red laser beam is directed on the mirror S3. From there it is redirected towards a lens. Again, as with the infrared laser, a diode (labeled D_{670}) is placed in the focus point of this lens, preceded by a pinhole to collect scattered light.

The data during the experiment are gathered by a LeCroy 8013A, containing two module 6810 AD-converters. Using these AD-converters, the LeCroy is capable of measuring up to 8 different signals simultaneously. In our case 4 signals are measured simultaneously: the output of the Kistler in the expansion chamber, the output of D_{670}, the output of D_{820} and the output of D_{REF}.

The LeCroy is controlled and operated using software installed on a PC. Via this program, called Catalyst, the data from all 4 signals can be saved in separate binary files (referred to as raw data files). These files are then used in the data-acquisition software. In this program, the signals, measured by the LeCroy are translated in a pressure signal, the transmission signals for light of both lasers and the corresponding extinction signals.

4.3 Analyzing measurements and results

An example of the signals measured is given by figure 22 where the pressure signal is shown together with the transmission of the 670 nm laserbeam and the 820 nm laserbeam. The experiments were performed with a Helium/Water mixture with an initial temperature of 293.4 K and a relative humidity of 0.85.

Unlike the theoretical pressure signal from chapter 3, the pressure signal shown in figure 22 contains perturbations and noise. The first perturbation can be seen at $t \approx 2 \cdot 10^{-3}$ s. This is the result of the opening of the magnetic valve. The second perturbation at $t \approx 4 \cdot 10^{-3}$ s is the effect of the latent heat. In real pressure signals, the effect of an increase in temperature (due to the latent heat) will immediately be translated into an increase in pressure, which results in a change in the transmitted light[4].

---

[3] The main reason for extinction is the scattering of light by droplets. Scattering will be omnidirectional, so a small part of the light will be scattered in the direction of the transmitted beam.

[4] In the analysis of the experiments, the effect of latent heat was found to be small enough to be discarded.

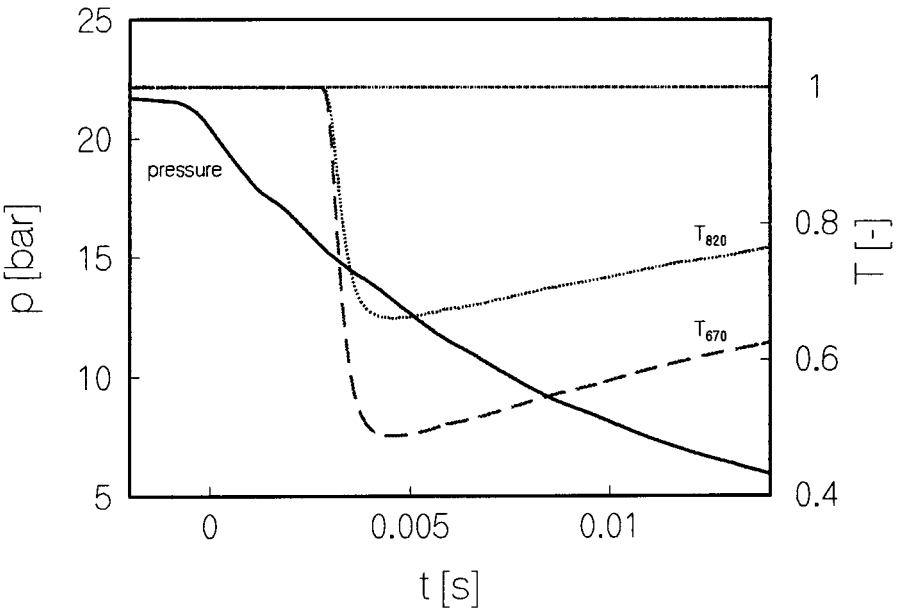

Figure 22 : Example of the transmission of the 670 nm wavelength and the 820 nm wavelength during an expansion using a Helium / Water gas / vapor mixture with initial pressure p_0 = 22 bar, initial temperature T_0 = 294 K and an initial relative humidity RH_0 = 0.85.

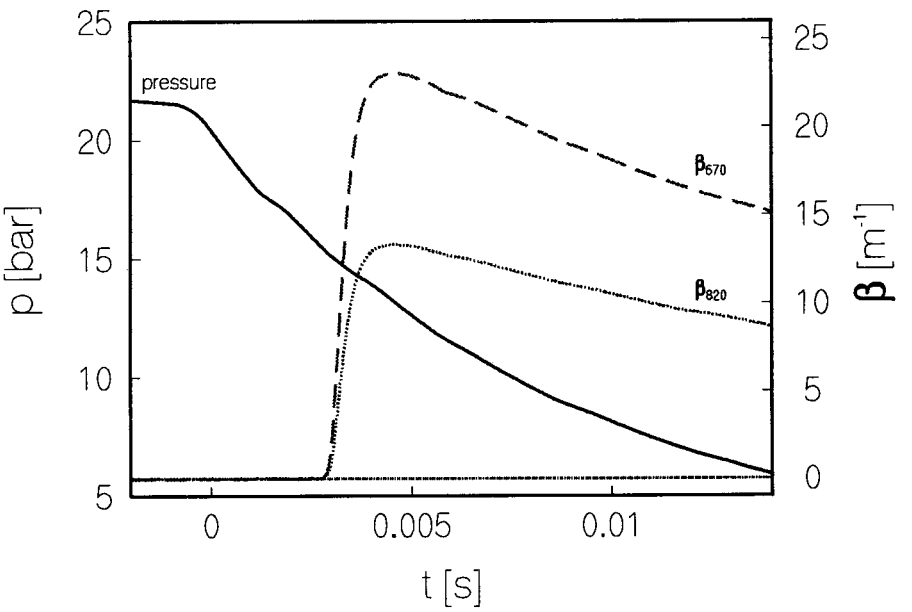

Figure 23 : Example of the extinction of the light of the 670 nm laser and the 820 nm laser during an experiment using a Helium / Water gas / vapor mixture with initial pressure p_0 = 22 bar, initial temperature T_0 = 293.4 K and an initial relative humidity RH_0 = 0.85.

simulation (since it is already in the pressure signal). The extinction signals for the experiment of figure 22 are given in figure 23.

The experiment can be simulated by using the pressure signal from figure 22 as the input of the numerical simulation program (chapter 3) together with the known initial conditions. The resulting (theoretical) extinction signal β_{670} of this experiment is shown in figure 24, together with the measured extinction signal β_{670} (the result for β_{820} is the same, so it is not shown).

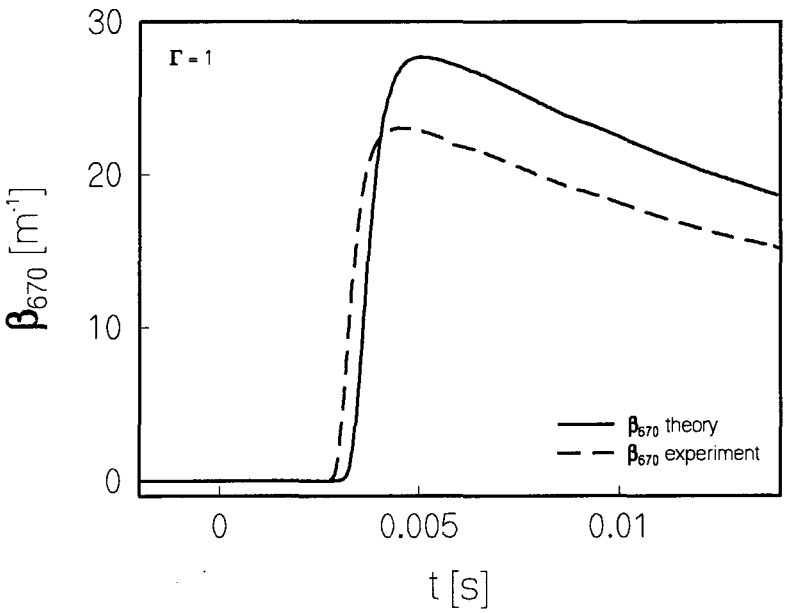

Figure 24 : The theoretical and experimental extinction for light of the 670 nm laser for the experiment of figure 22, using the CNT and Γ=1

From this figure it can be seen that the extinction signal β_{670} of the experiment starts before the theoretical extinction signal β_{670}. From this it can be concluded that the experimental nucleation rate is higher then the nucleation rate predicted by the CNT. Furthermore, the maximum of the extinction signal β_{670} is lower than the theoretical extinction signal β_{670}[5].

The nucleation rate from the CNT used in the simulation of the experiment is now multiplied by a factor Γ. If Γ is larger then unity, the net

[5] The maximum of the extinction is determined by the growth model (which makes assumptions that are not always valid) and by the surface tension γ, the diffusion coefficient D etc. The latter parameters are not exactly known.

result will be that the onset of the theoretical extinction β^{CNT} will shift to an earlier time. If Γ is lower then unity the result will be an opposite shift in time. Using this parameter Γ, the beginning of the theoretical extinction β^{CNT} can be matched with the beginning of the experimental extinction β^{EXP}. For the experiment shown figure 24, a value Γ=200 was found (figure 25).

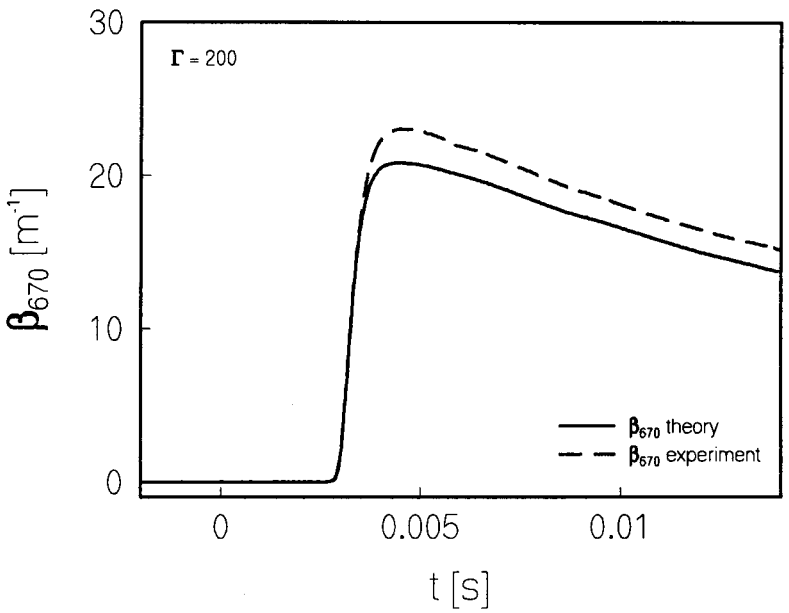

Figure 25 : The theoretical and experimental extinction for light of the 670 nm laser for the experiment of figure 22, using the CNT and Γ=200.

From the analysis in chapter 3 it is known that the beginning of the extinction is determined mainly by the nucleation rate. Since the nucleation rate is the quantity of interest, only the beginning of the extinction signal is matched. It can be noticed also, that the extinction signal after the maximum does not match the experimental extinction, which is caused by the uncertainties in the process parameters, the initial parameters and the growth model.

4.4 Influence of uncertanties

In chapter 3, the variation in the optical extinction was analyzed for a given variation in the vapor pressure p_{vap}, the diffusion coefficient D and the surface tension γ. Again variations in these parameters are considered, only now our interest is focused on the effect on Γ.

Table 1 The effect of changes in initial parameters and process parameters on the value of Γ

	Γ
0.99 $p_{v,0}$	280
1.00 $p_{v,0}$	200
1.01 $p_{v,0}$	120
0.99 γ	40
1.00 γ	200
1.01 γ	500
0.95 D	220
1.00 D	200
1.05 D	180
0.50 D	1000
1.00 D	200
2.00 D	40

The theoretical extinction signal of the experiment in figure 24 (using Γ=200) is considered as a reference. Next the simulation is repeated using the same Γ but with small variations on either $p_{v,0}$, γ or D. Finally Γ is varied until the beginning of the extinction signal matches the initial extinction signal. The results of the variations in $p_{v,0}$, γ and D are shown in table 1. For a Helium/Water mixture, the diffusion coefficient is taken from a general empirical fit [REID87]. From this fit it is known that for higher pressures, the value of the diffusion coefficient has an error ranging from 5%-50% [ROE95]. However, these uncertainties in the diffusion coefficient were only found by examining complex vapor molecules (e.g. carbon-hydrogens). For small molecules (e.g. water) it is assumed that the error is approximately 5%.

From table 1 it is clear that the errors in the initial parameters produce a logarithmic effect on Γ, that is they multiply the value of Γ by some constant rather then increase it by some constant. Thus the total error in Γ is found by summing up all multiplication factors. Assuming the diffusion coefficient D has only a small (5%) error then the total error on log Γ is ± log 10. If the diffusion coefficient has a larger error (50%) then the total error on log Γ is: ± log 15.

The experiments were analyzed using the numerical simulation from the previous chapter. By varying Γ, the theoretical extinction signal was matched with the measured extinction signal. Again, this was done by looking only at the beginning of the extinction signals.

Two series of experiments were done, using Helium as carrier gas. For the first series (referred to as HE30) initially 30µl of water was injected for each experiment. This yields a relative humidity ranging from 80% to 90%. For the second series (referred to as HE10), initially 10µl of water was injected for each experiment (yielding a relative humidity ranging from 50% to 60%).

The resulting Γ's for both series are presented in figures 26 and 27 as a function of *condensation temperature* (the condensation temperature is defined as the temperature at the maximum of the nucleation rate) together with values found in the literature (table 2 shows the experiment number, some initial conditions and the corresponding values of Γ). The theoretical extinction was computed for two different nucleation models, the classical nucleation model (Γ_{CNT}) and the semi-phenomenological nucleation model (Γ_{SPT}).

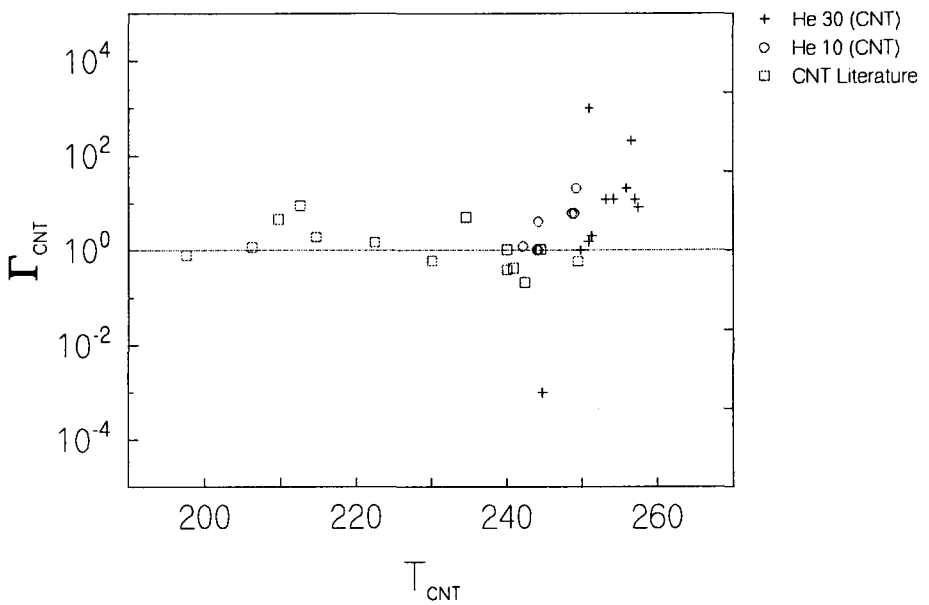

Figure 26 : The correction factor Γ versus the nucleation temperature for the classical nucleation theory (CNT).

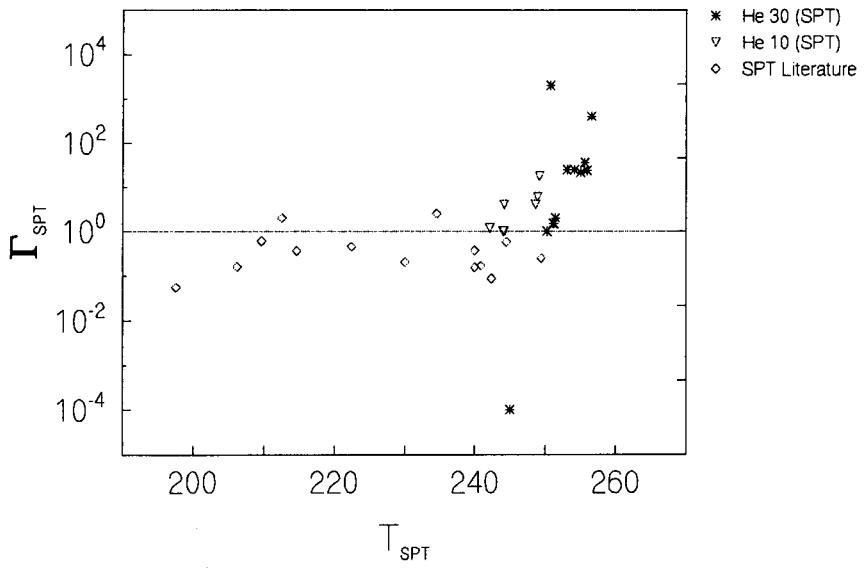

Figure 27 : The correction factor Γ versus the nucleation temperature for the semi-phenomenological theory (SPT).

Figures 26 and 27 also show the values for Γ computed using experimental nucleation rates found in the literature [LOO95][6]

[6] Note that the condensation temperature defined in the literature can be different.

Table 2 Resulting Γs of the EH series using two nucleation different models.

exp.no.	p_0 [bar]	$p_{v,0}$ [kPa]	Γ_{CNT}	$T_{cond,CNT}$ [K]	Γ_{SPT}	$T_{cond,SPT}$ [K]
1006	41,3	2,06	12	253	25	253
1007	41,8	2,21	12	254	25	254
1008	80,5	1,71	1000	251	2000	251
1009	80,2	2,09	1	250	1	250
1012	53,8	2,22	0,001	245	0,0001	245
1013	62,3	2,12	2	251	2	251
1014	61,4	2,13	2	251	1,5	251
1015	61,3	2,11	1,5	251	1,5	251
1016	21,7	2,24	200	257	400	257
1017	21,7	2,27	20	256	22	255
1019	6,8	2,15	8	258	24	256
1020	7,03	2,12	12	257	36	256

From figures 26 and 27, it can be concluded that most Γ-values from the HE30 and HE10 series are in agreement with the values found in the literature, considering the uncertainty of one order in Γ. Only 3 three experiments show a significant different value of Γ. Also it can be seen that a horizontal line can be drawn if the experimental values for Γ are combined with the literature values for Γ (within the margin of error).

The effect of pressure on Γ is shown in figure 28. From this figure an it can be concluded that for Helium as a carrier gas, Γ is independent of the pressure (within its margin of error). Again, three points are in disagreement with this result.

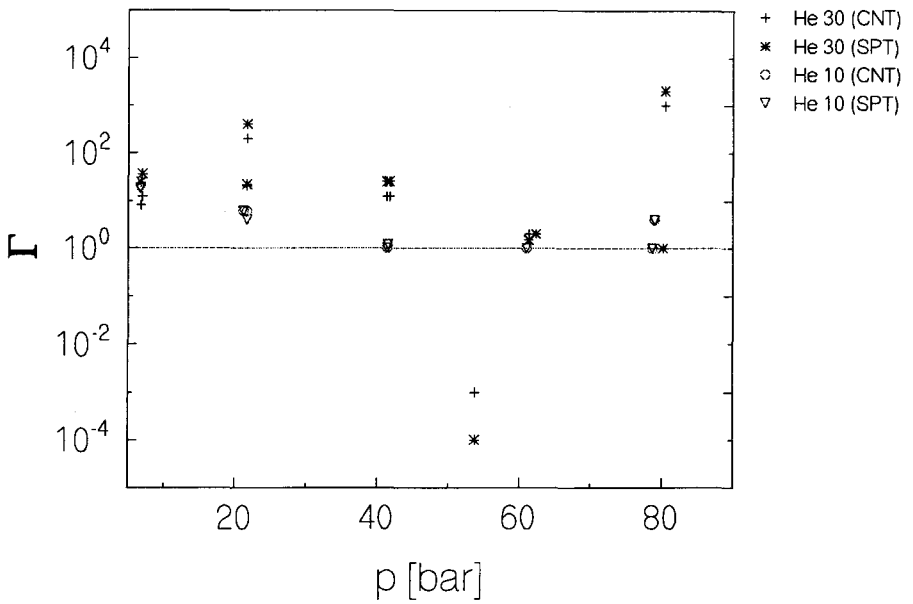

Figure 28 : The correction factor Γ versus the initial pressure for two different nucleation models (CNT and SPT).

Table 3 Resulting Γ's of the HE10 series using two different nucleation models.

exp.no.	p_0 [bar]	$p_{v,0}$ [kPa]	Γ_{CNT}	$T_{cond,CNT}$ [K]	Γ_{SPT}	$T_{cond,SPT}$ [K]
1030	79,0	1,43	6	244	4	244
1031	78,7	1,53	1,2	244	1	245
1032	61,0	1,54	1	244	1	245
1033	41,5	1,31	1,2	242	1,2	243
1034	41,4	1,46	1	244	0,9	244
1035	21,2	1,69	6	249	6	249
1036	6,8	1,46	18	248	16	248
1042	21,7	1,66	4	249	4	249

DISCUSSION & CONCLUSIONS

In this report two nucleation theories where presented. One theory is the well known classical nucleation theory. The other theory is the recently developed semi-phenomenological theory. For water, the vapor used in the experiments described in this report, both theories predict approximately the same nucleation rates.

The experimental method (a expansion cloud chamber) used to obtain the nucleation rate is based on the measurement of extinction of light. This is an indirect method, however it is very sensitive. From the extinction, the nucleation rate can be found by comparing the measured extinction signal with a theoretical extinction signal for a given nucleation model and droplet growth model. For this purpose, a numerical simulation of the experiment was developed.

A theoretical analysis was performed using the numerical simulation of the expansion cloud chamber. Parameters investigated were the initial parameters T_0 and $p_{v,0}$ and the process parameters D and γ. From this analysis it is clear that small deviations in T_0, γ and $p_{v,0}$ yield the largest effect on the extinction signals (the variations were chosen according to estimated uncertainties in the experimentally measured values). Since small variations yield a large effect on the extinction it is obvious that an accurate determination of the initial vapor pressure an the initial temperature is essential. Furthermore, the empirical temperature dependence of the surface tension needs to be known with more accuracy.

The effect of the diffusion coefficient should be considered with caution. Since there were no known specific empirical relations found for the diffusion coefficient for Helium/water gas/vapor mixtures, a general empirical relation was used [REI87]. From this relation it is known that the diffusion coefficient for complex vapor molecules has an uncertainty ranging from 5% at low pressures to approximately 50% at high pressures [ROE95]. However, this was only verified for complex vapor molecules (e.g. nonane). For water (a rather simple molecule), it is assumed that the error in D ranges from 5% to 10%.

The numerical analysis performed on a theoretical pressure signal (chapter 3) was repeated for a measured pressure signal. This was done to investigate the effect of these variations in the correction factor Γ for the nucleation rate. The result was that the error in Γ could best be expressed as a multiplication by a constant factor. This indicates that β is very sensitive to changes in the initial parameters and the process parameters.

Also important is the effect of a change in the diffusion coefficient D on the value of Γ. For small variations (5%) the change in Γ is negligbly. For this error

in D the total uncertainty of Γ was set to a factor 10. However in the worst case (a 50% error in D) the total error in Γ would only increase by a factor 5. This confirms that Γ is mostly determined by the nucleation rate.

The experiments were analyzed using the numerical simulation in order to obtain the correction factor Γ for the theoretical nucleation rate. This was done for two series of experiment using a helium/water gas/vapor mixture of different composition. Both series were analyzed with two different nucleation models (CNT and SPT) yielding a correction factor Γ^{CNT} and Γ^{SPT}. Comparison of the experimental Γ's with values found in the literature showed acceptable agreement for most values of Γ. It was also found that the value of Γ was (within the margin of uncertainty) indepent of pressure.

BIBLIOGRAPHY

[ABR74] Abraham, E. E., *Homogeneous Nucleation Theory*
Academic Press (1974)

[BEC35] Becker, R & Döring, W.
Ann. Phys., 24, 719 (1935)

[GYA82] Gyarmathy, G., *Zur Wachstumgeschwindigkeit kleiner Flussigkeitstropfen in einer ubersattigten Atmosphare*
ZAMP Vol. 14, n° 3, pag. 280 (1963)

[KAL95] Kalikmanov, V. I., *Statistical Thermodynamics of liquids*
lecture notes on the course 'statistical thermodynamics of liquids'
Eindhoven University of Technology (1995)

[KAT77] Katz, J. L. & Wiedersich, H.
J. Colloid Interface Sci., 61, 351 (1977)

[KER69] Kerker, M., *The Scattering of Light and other Electromagnetic Radiation*
Clarkson Coll. of Techn.: Dept. of Chem.
Potsdam N.Y. Academic Press (1969)

[LAN69] Landau, L. D. & Lifshitz, E. M., *Statistical Physics*
Pergamon, Oxford (1969)

[LOO95] Looijmans, K. H. N, *Homogeneous nucleation and droplet growth in the coexistence region of n-alkane/methane mixtures at high pressures*
Eindhoven University of Technology (1995)

[REI87] Reid, R. C., Prausnitz, J. M. & Poling, B.E, *The properties of Gases and Liquids*
McGraw-Hill Book Company, New York (1987)

[ROE95] Roelands, M. {title}
master thesis
Eindhoven University of Technology (1995)

[ZEL43] Zeldovich, Ya. B.
Acta Physiocochim, URSS, 18, 1 (1943)

DESCRIPTION OF THE SIMULATION PROGRAM

Introduction

The simulation program WILSON32.FOR was created as a reference for future simulations. It therefore inhibits a fundamentally different layout than normal, single purpose simulation programs. The main reason for this was that the program should be independent of various nucleation models, growth models etc. To achieve this a separate layer was inserted between the main program, describing the actual simulation and the individual models describing nucleation, growth etc.

Requirements

An executable image of WILSON32.FOR can be created by compiling and linking all necessary .FOR files. The files necessary are:

- WILSON32.FOR	main simulation program
- ID.FOR	describing the ideal equation of state
- IDNUCL.FOR, IDNUCLV.FOR	describing the nucleation theory (CNT or SPT)
- IDGROW.FOR	describing the growth model (Gyarmathy)
- IDPROC.FOR	describing parameters of various substances

The first two characters of the model files (ID) were introduced as a naming convention to indicate that the files are used together with the ideal equation of state.

General description of the file layout

The interior of each *model file* can be roughly divided in three areas. The top of the file contains a large comment block, describing the call to all the functions and subroutines implemented in the rest of the file, in the same order as they appear in the rest of the file. This comment block was created to speed up the search for a given function or subroutine (in most cases the programmer

only wants to know how to call a given function or subroutine).

Below this comment block the implementation of all *model dependent* functions and subroutines are given. These are functions and subroutines that are dependent on a specific model. A direct call to these functions outside the file in which they are implemented should be avoided, in order to preserve the model independence.

The last part of the file is devoted to the so called *interface routines*. These are the routines that can be called freely from within other model files and the main program. The interface functions form a standard set of functions that are called whenever communication between the main program and the models takes place. They are also used for communication between the model files.

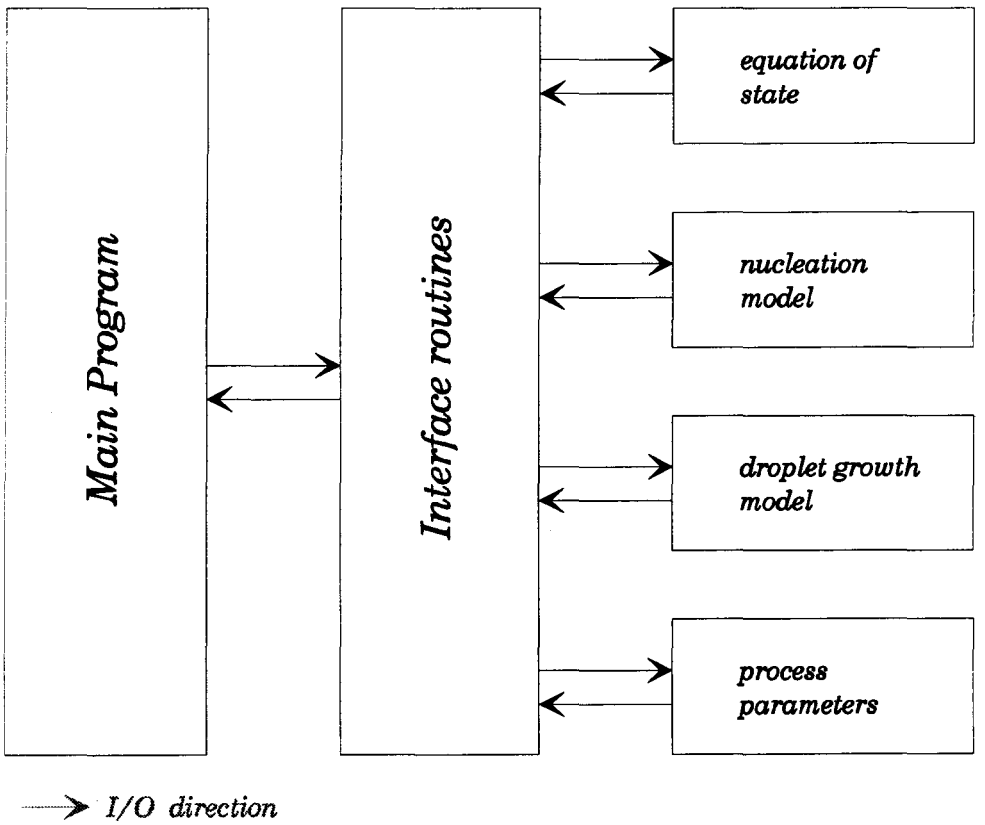

Figure A1 : Schematic view of the communication between the main program file and the model files.

An example: assume the main program wishes to compute the latent heat of the condensing liquid. Then it calls the interface routine `GetLHeat(..)` which is declared as

```
DOUBLE PRECISION FUNCTION GetLHeat(p,T,V,y,Vliq,x).
```

The interface routine in its turn will call the model dependant function `IDLHeat(..)` which computes the latent heat for water. This function is declared as

```
DOUBLE PRECISION FUNCTION IDLHeatH2O(T).
```

Now it is be possible to call `IDLHeatH2O(..)` directly, but the advantage of the interface routines becomes visible if a new fit is introduced for the latent heat, depending on both temperature and pressure.

If `IDLHeatH2O(..)` was called directly, the programs source has to be corrected everywhere the function is called. The larger a program tends to become, the more difficult this will be, since one or more function calls will be overlooked.

Now with this interface routine, only the call to `IDLHeatH2O(..)` was made inside the interface routine and this will now be the only routine that needs to be corrected. Since all other parts of the program call the interface routine, they will automatically use the new version of `IDLHeatH2O(..)`.

Running the simulation program

The program `WILSON32.FOR` accepts its input from a file. This file is called `WILSON.USR` and contains plain ASCII. The general layout of this file is:

```
//
// lines of comments
//

[COMMAND]
[THEO]|[REAL]

//
// data
//

...

[END]
```

The program `WILSON32.FOR` starts reading the input file after it has encountered a section header `[COMMAND]`. All text preceding this header will be skipped and can be used as an area for comments (the `//` are not necessary, they are only added to improve readability for the user).

The section header [COMMAND] will trigger the start of the simulation.

From this point on WILSON32.FOR expects input according to a predefined format. First either a section header [THEO] (indicating a theoretical pressure signal should be used) or [REAL] (indicating the pressure signal is read from an input file) is expected. After that, depending on the choice of [THEO] or [REAL], initial parameters are expected. The parameters are all preceded by a line of comment, describing what the next parameter is. An example of a WILSON.USR input file is given at page 57 and the following ones.

```
%
%  All lines preceding a [COMMAND] are ignored and can be used for comment.
%  The %-sign is not necessary but it improves the readability of the .USR
%  file.
%
%  Each simulation is preceded by a section-header named [COMMAND]. Then a
%  header [THEO] (if a theoretical pressure signal is to be used) or a
%  header [REAL] (if a pressure input file is to be used) must be given.
%  Then the data must be given in the format:
%
%   1. a line of comment (used to describe the next value)
%   2. value of a parameters
%
%  input for [THEO]
%
%    1. tau-value
%    2. time step
%    3. minimum value of chi
%    4. minimum number of droplets
%    5. correction gamma for nucleation
%    6. correction gammadiff for diffusion coefficient
%    7. correction gammasigma for surface tension
%    8. output file (preferably .ASC)
%    9. statistics file (.STA)
%   10. log file (.LOG)
%   11. component number #1
%   12. component number #2
%   13. initial pressure
%   14. final pressure
%   15. initial temperature
%   16. initial vapor pressure
%   17. number N of droplet distributions to save during the simulation
%   18. time of save and output file of droplet distribution 1..N
%
%  input for [REAL]
%
%    1. time step
%    2. minimum value of chi
%    3. minimum number of droplets
%    4. correction gamma for nucleation
%    5. correction gammadiff for diffusion coefficient
%    6. correction gammasigma for surface tension
%    7. pressure input file
%    8. output file (preferably .ASC)
%    9. statistics file (.STA)
%   10. log file (.LOG)
%   11. component number #1
%   12. component number #2
%   13. relative humidity RH (in %)
%   14. temperature HUMICAP (in V)
%   15. number N of droplet distributions to save during the simulation
%   16. time of save and output file of droplet distribution 1..N
%
%  The program stops when it encounters a [END] section.
%
%  Note: All filenames must be given using a full name (NAME+EXTENSION)
%
%  Note: Time of save and output file for the droplet distributions must
%        be given on separate lines. No comment lines allowed between
%        pairs of (time, output file).
%
%        Example:
%
%        C---- number of droplet distributions to save
```

```
%         3
%         C---- time of save and output file of droplet distributions
%         1D-3
%         1msec.asc
%         1.2D-2
%         12msec.asc
%         2D-2
%         20msec.asc
%
%  Note: Between two section headers [COMMAND] there is room for additional
%        comments (these lines are ignored)
%

%
%  Example of a theoretical simulation
%
[COMMAND]
[THEO]
C---- tau
2D-2
C---- time step
1D-5
C---- minimum value of chi (above this value data are saved)
1.0
C---- minimum number of droplets
1000.0
C---- correction factor for nucleation
1.0
C---- correction factor for the diffusion coefficient
1.0
C---- correction factor for the surface tension
1.0
C---- output file
out.asc
C---- statistics file
out.sta
C---- log file
out.log
C---- component #1 : Water
16
C---- component #2 : Helium
19
C---- initial pressure
5D5
C---- final pressure
2D5
C---- initial temperature (K)
295
C---- vapor pressure
2000
C---- number of droplets distributions to save
0
C---- values of t and filename for droplet distribution

%
% Example of a simulation using an input file
%
[COMMAND]
[REAL]
C---- time step
1D-5
C---- minimum value of chi (above this value data are saved)
1.0
C---- minimum number of droplets
```

```
1000.0
C---- correction factor for nucleation
1.0
C---- correction factor for the diffusion coefficient
1.0
C---- correction factor for the surface tension
1.0
C---- pressure input file
expresu.asc
C---- output file
out.asc
C---- statistics file
out.sta
C---- log file
out.log
C---- component #1 : Water
16
C---- component #2 : Helium
19
C---- relative humidity
0.8223
C---- temperature environment (K)
294.2
C---- number of droplets distributions to save
0
C---- values of t and filename for droplet distribution

[END]
```

TURBULENCE IN THE EXPANSION CLOUD CHAMBER

During an adiabatic expansion, the flow of gas/vapor changes for laminar to turbulent. This is effect is shown in figure B.1 where the optical signals of an expansion using only nitrogen (no vapor component). It is most likely caused by the geometric form of the expansion cloud chamber (the expansion chamber is shaped in a diamond form at the top which gradually transforms in a circular form at the bottom).

The appearance of turbulence was discovered due to the fact that the optical detection method is very sensitive to small deviations of the main beam (due to the pinholes in front of the diodes). This is the main cause for the loss in signal. It was observed that if the pinholes are removed, the loss in signal decreases by a factor 3 to 5.

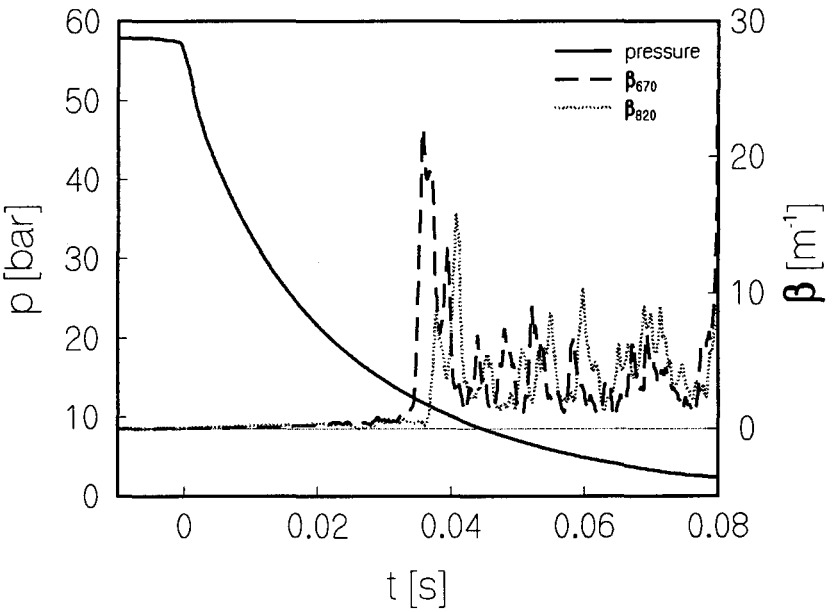

Figure B1 : The extinction β_{670} and β_{820} for a expansion using only nitrogen.

The onset point of the turbulence was found to be nearly independent of the pressure. The amount of signal loss however was both dependant on the pressure and the speed of the expansion. The turbulence is also dependent on the gas type (for helium the effects were less severe then for nitrogen).

Several methods were tried to prevent the laminar flow to develop into a

turbulent flow. The expansion chamber was enlarged by inserting a 2 cm wide ring at the top of the expansion chamber. This yielded a shift of the onset of the turbulence to an *earlier* time. Also rotating the expansion chamber was without any significant result. Until now, no satisfying explanation has been found for the appearance of turbulence.

PRESSURE CALIBRATIONS

Description and results of the calibration of the Kistler sensitivity

The high pressure sensitivity of the Kistler was measured using the following method. First: vacuum chamber is disconnected. Next, the expansion chamber is filled with pure gas. Then a dry experiment (an expansion using only a carrier gas) is done.

The pressure signal of the Kistler is translated by the LeCroy into a bit change. Using a conversion program (ICONVERT), the raw data file of the pressure signal can be converted into an ASCII file containing only the bit change of the LeCroy. With the known initial pressure and the environment pressure, the pressure fall can now be related to a bit fall, yielding the sensitivity of the Kistler.

The low pressure sensitivity of the Kistler was measured using the same method only now the vacuum chamber was not disconnected. This is wrong, which explains the difference in sensitivity of nearly 4% between the high pressure and low pressure calibration. In the analysis of the experiments only the high pressure sensitivity was used.

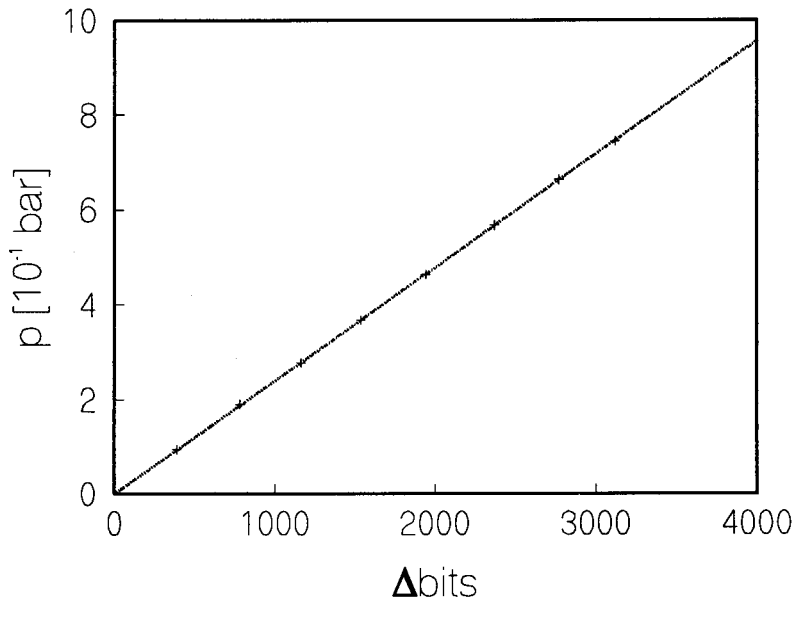

Figure C1 : High pressure

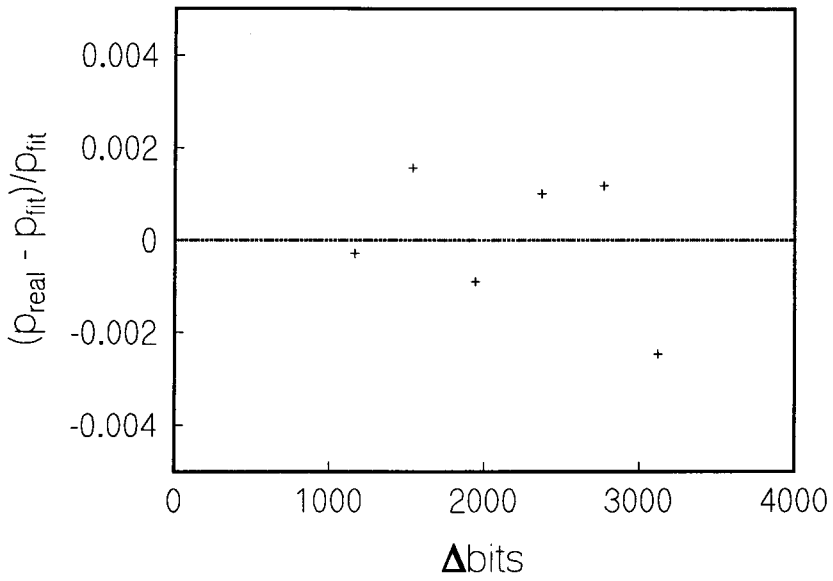

Figure C2 : High pressure gauge for the Kistler in the expansion chamber.

Results of the calibration of the Druck EV

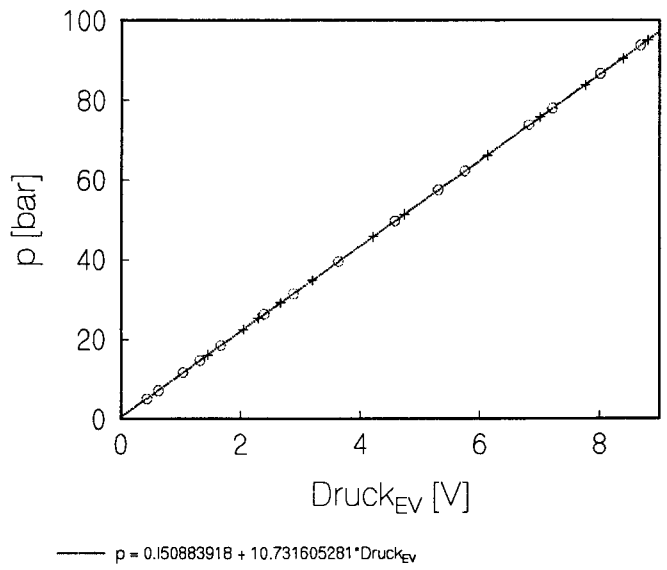

Figure C3 : High pressure gauge for the Druck EV.

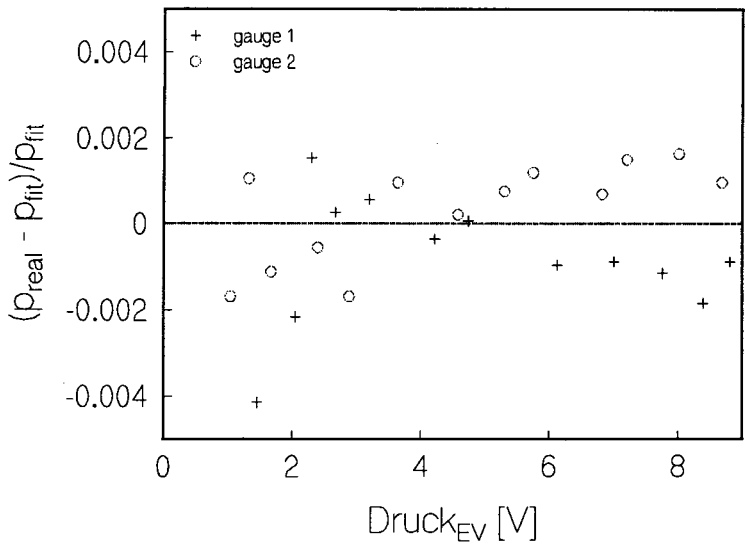

Figure C4 : Relative errors for the high pressure gauge of the Druck EV.

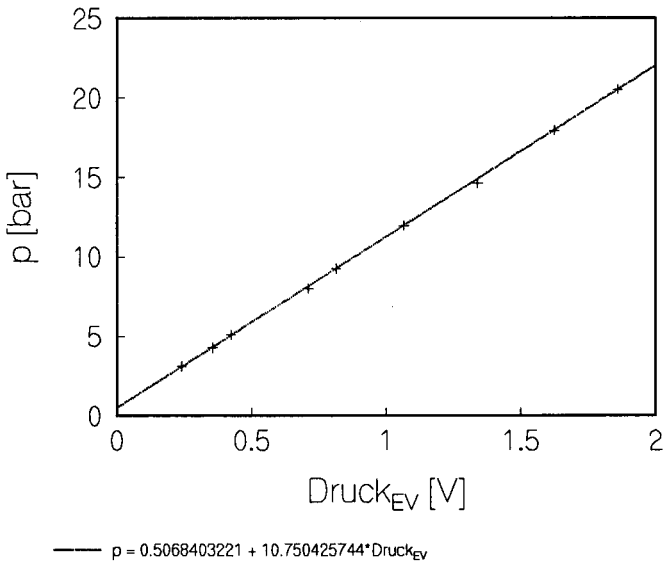

Figure C5 : Low pressure gauge for the Druck EV.

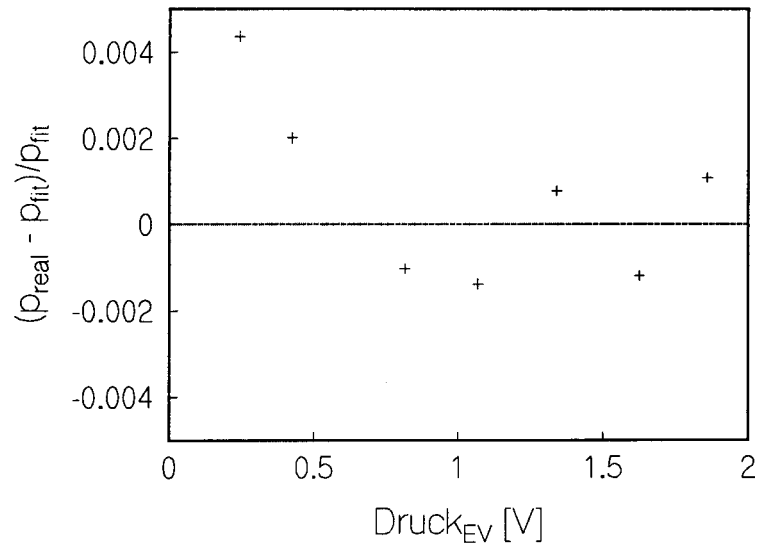

Figure C6 : Relative errors for the low pressure gauge of the Druck EV.

THE FISHER DROPLET MODEL

The Fisher droplet model has its origin in statistical mechanics. The approach is to find the grand potential Ω_n of a n-cluster, in order to derive some expression for ΔG_n. From statistical thermodynamics it is known that Ω is related to the grand partition function Ξ of an open system (μ-V-T).

$$\Omega(\mu, V, T) = -k_B T \ln \Xi \tag{A.1}$$

The grand partition function of an open system is related to the partition function Z_N of a system with fixed number of particles (N-V-T) by the relation [LAN69]

$$\Xi = \sum_{N \geq 0} \lambda^N Z_N \tag{A.2}$$

where $\lambda = e^{\beta\mu}$ is activity and the partition function Z_N can be found from the relation

$$Z_N = \frac{1}{N!} \int e^{-\beta H(\vec{r}_1, \ldots, \vec{r}_N, \vec{p}_1, \ldots, \vec{p}_N)} d\Gamma \tag{A.3}$$

were H is the Hamiltonian of the system, describing the kinetics and the interaction between the N particles in a volume V at temperature T. If the interaction potential is independent of the momentum of the particles then the momentum part of the partition function can be split from the configurational part and solved. The solution of the momentum part yields

$$\frac{1}{2\pi\hbar} \int_{-\infty}^{\infty} e^{-\frac{\vec{p}_i^{\,2}}{2mk_BT}} d\vec{p}_i = \frac{1}{\Lambda^{3N}} \tag{A.4}$$

where $\Lambda = (2\pi\hbar^2/m_1 k_B T)^{1/2}$ is the thermal De Broglie wavelength. Z_N can now be written as

$$Z_N = \frac{1}{N! \Lambda^{3N}} Q_N \tag{A.5}$$

with Q_N the so called *configuration integral*, given by

$$Q_N = \int e^{-\beta(U_N + U_{N,ext})} d\vec{r}_1 \ldots d\vec{r}_N \,. \qquad (A.6)$$

This integral describes all the possible configurations in space of N molecules, for a given interaction potential $U_N+U_{N,ext}$.

In order to find the grand partition function Ξ, the Hamiltonian of the n interacting vapor molecules forming the cluster needs to be known. With H known the energy eigenvalues of the system can be found and the configuration integral can be solved. However, an easier approach is to define the form of the energy eigenvalues based on simple physical reasoning.

Assume the most simple form of interaction between molecules: the square well potential (figure D.1). A vapor molecule can only be tied to its neighbor if the distance is less than σ. If it is tied by a single molecule it gains an amount ε_0 of energy. If it is tied by a cluster then the average energy gain e_0 will approximately ε_0 times the average number of neighbors. The total binding energy E_0 per molecule now is $\frac{1}{2}e_0$, in order to prevent double count when computing the total binding energy. So the energy needed for the formation of an n-cluster out of n vapor molecules should be proportional to nE_0.

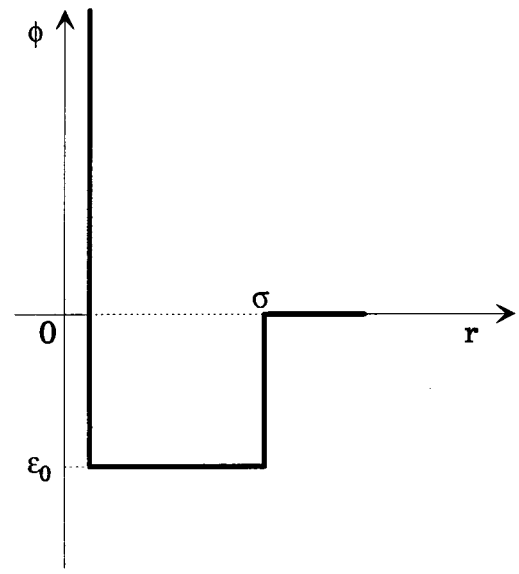

Figure D1 : the square well potential

On the other hand, forming a cluster can only be done by forming a surface. So an amount of work W_n is needed. It is assumed that the amount of work needed to form a surface is proportional to the surface s_n of the n-cluster, or $W_n=ws_n$. Now the potential energy U_n of the n-cluster can be written down, yielding

$$U_n = -nE_0 + W_n = -nE_0 + ws_n \,. \qquad (A.7)$$

In the Fisher droplet model the gas is assumed to have a distribution of clusters of various sizes. These clusters are considered to be ideal, that is, there is no intercluster interaction. Using this assumption, equation () can be used to calculate the configuration integral of the clusters. Since there is no interaction, the result will be trivial.

Now again, for the clusters it is possible to create a configuration integral. This time, there is a interaction between the molecules of the cluster, so using (A.7), the configuration integral for the n vapor molecules forming an n-cluster is given by

$$q_n = \frac{1}{n!} \int e^{-\beta U_n} d\vec{r}_1 \ldots d\vec{r}_n \,. \tag{A.8}$$

Equation (A.8) can be used to express the grand partition function in an exponential form [KAL95]. The final result is

$$\Xi = \exp\left[\sum_{n=1}^{\infty} q_n z^n \right] \tag{A.9}$$

where $z = e^{\beta\mu}/\Lambda^3$ denotes the fugacity. Since Ξ is related to the grand potential Ω by means of equation (A.1) and using the thermodynamic relation $\Omega = -pV$, the equation of state can be expressed as a power series

$$\frac{P}{k_B T} = \sum_{n=1}^{\infty} \left(\frac{q_n}{V} \right) z^n \,. \tag{A.10}$$

Using the configuration integral to compute the average number of particles $\langle N \rangle$ the number density $\langle N \rangle / V = \rho$ now becomes

$$\rho = \sum_{n=1}^{\infty} n \rho_n = \sum_{n=1}^{\infty} n \left(\frac{q_n}{V} \right) z^n \,. \tag{A.11}$$

To compute q_n, the configuration integral (A.8) is rewritten using a translation of the origin to the center of mass of the cluster and a representation in terms of the surface s_n of the n-cluster. The result yields

$$q_n = V\sum_{s_n} g(n,s_n)e^{n\beta E_0 - \beta w s_n}, \qquad (A.12)$$

where $g(n,s_n)$ describes the number of different configurations yielding the same surface for the n-cluster. The factor $g(n,s_n)$ has a strong relation with the entropy of an n-cluster.

In order to find an expression for $g(n,s_n)$ the entropy of an n-cluster S_n is computed. Like (A.7) the entropy S_n of the n-cluster is written as the sum of a bulk term and a surface term.

$$S_n = nS_0 + \omega s_n \qquad (A.13)$$

Here S_0 is the liquid bulk entropy per molecule. The factor ω depends on the number of possible configurations having the same surface. A relation between $g(n,s_n)$ and S_n can be found by calculating the so called *configurational entropy* which is related to the configurational Helmholtz free energy by

$$F_n^{conf} = -k_B T \ln q_n \qquad (A.14)$$

Inserting (A.12) in (A.14) yields

$$S_n = k_B\left[\ln q_n - \beta \frac{1}{q_n}\frac{\partial q_n}{\partial \beta}\right] \qquad (A.15)$$

where the second term on the r.h.s. can be expressed as $nE_0 - \langle W_n \rangle$ ($\langle W_n \rangle$ is the thermal average of the energy needed to create the surface of an n-cluster). Using this, equation (A.15) can be rewritten to

$$S_n(\beta) = k_B[\ln q_n - \beta n E_0 + \beta \langle W_n \rangle]\,. \qquad (A.16)$$

Comparing (A.13) to (A.16) results in an expression for the bulk entropy S_0 [KAL95]. Using the function $G_n(\beta)$, defined as

$$G_n(\beta) = \sum_s g(n,s_n)e^{-\beta w s_n} = \frac{q_n}{V}e^{-\beta n E_0} \qquad (A.17)$$

and equation (A.16) it follows that

$$S_0(\beta) = k_B \lim_{n\to\infty}\left[\frac{1}{n}\ln G_n(\beta)\right] \qquad (A.18)$$

The smallest possible surface in three dimensions is given by the surface of a sphere, which is proportional to $n^{2/3}$. More generally, the smallest possible surface is proportional to $n^{1-(1/d)}$ where d is the spatial dimension. The largest possible surface is proportional to n (a chain in three dimensions). In other words $a_1 n^{1-(1/d)} \le s_n \le a_2 n$, where a_1 and a_2 are some arbitrary factors. Using this result combined with the knowledge that G_n only contains positive terms leads to

$$\max_{s_n}\left\{g(n,s_n)e^{-\beta w s_n}\right\} \le G_n(\beta) \le a_2 n \max_{s_n}\left\{g(n,s_n)e^{-\beta w s_n}\right\} \qquad (A.19)$$

Now assume the maximum of G_n is attained for some value $s_n=\langle s_n\rangle$ then this value $\langle s_n\rangle$ is the most probable surface area or the *mean surface*. Since at low temperatures there is a tendency to form compact objects, this mean surface $\langle s_n\rangle$ will almost certainly increase with n more slowly than n, so it can be written as a power of n. On the other hand this power of n is limited by the power that describes the most compact object in the given dimension (which is $n^{1-1/d}$). So $\langle s_n\rangle$ can be written generally as

$$\langle s_n\rangle = a_0 n^{\sigma} \qquad (A.20)$$

where $1-1/d \le \sigma < 1$. Now $g(n,s_n)e^{-\beta w s_n}$ is sharply peaked around the value $\langle s_n\rangle$, since $g(n,\langle s_n\rangle)$ will be very large. So the major contribution to the sum in (?) will come from the term containing $\langle s_n\rangle$. Using (?) this leads to

$$\ln G_n(\beta) = \ln g(n,\langle s_n\rangle) - \beta w \langle s_n\rangle + O(\ln n) \qquad (A.21)$$

For very large clusters ($n\to\infty$), the value $\langle s_n\rangle/n$ will go to zero (since $\sigma<1$). So for large clusters

$$\lim_{n\to\infty} \frac{1}{n} G_n(\beta) = \lim_{n\to\infty} \frac{1}{n} g_n(n,<s_n>) \qquad (A.22)$$

holds, stating that the surface contribution to the entropy becomes negligible. Using (A.18) and (A.22) it can be seen that for large clusters (n->∞) the bulk term of the entropy, nS_0, can be related to $k_B \ln g(n,<s_n>)$. For smaller clusters there is a difference that can be assigned to the surface term in the entropy (A.13).

$$k_B \ln g(n,<s_n>) - nS_0 \approx \omega <s_n> \qquad (A.23)$$

So now ln $g(n,s_n)$ is known.

Expressing O(ln n) as $-\tau \ln n + \ln q_0$, equation (A.21) can be rewritten, yielding

$$\ln G_n(\beta) = n\frac{S_0}{k_B} - \beta(w - \omega T)<s_n> - \tau \ln n + \ln q_0 \qquad (A.24)$$

Now the problem was to approximate the configuration integral in (?). Rewriting the result (A.23)

$$\ln g(n,s_n) = \frac{nS_0}{k_B} + \frac{\omega <s_n>}{k_B} \qquad (A.25)$$

and inserting $<s_n>=a_0 n^\sigma$ it is possible to write the quotient q_n/V as

$$\frac{q_n}{V} = n^{-\tau} q_0 \left\{ e^{\beta E_0 + S_0/k_B} \right\}^n \cdot \left\{ e^{-a_0 \beta (w - \omega T)} \right\}^{n^\sigma} \qquad (A.26)$$

Inserting the result in the equation of state, the latter on can be rewritten to

$$\frac{p}{k_B T} = \Pi(\beta, z) = q_0 \sum_{n=1}^{\infty} y^n x^{n^\sigma} n^{-\tau} \qquad (A.27)$$

where x (a temperature variable) and y (a variable proportional to the activity) are given by

$$x = e^{-a_0 \beta (w - \omega T)} \tag{A.28}$$

$$y = z\, e^{\beta E_0 + S_0/k_B} \tag{A.29}$$

Using the same notation ρ can be expressed as

$$\rho = q_0 \sum_{n=1}^{\infty} n^{1-\tau} y^n x^{n^\sigma} \tag{A.30}$$

so the number density of n-clusters is given by

$$\rho_n = q_0 y^n x^{n^\sigma} n^{-\tau} \tag{A.31}$$

The function $\Pi(\beta,z)$ is a so called *generating function*, that can be used to derive various thermodynamic quantities by simply taking a derivative of $\Pi(\beta,z)$ and multiplying it by z. Some examples:

$$\rho = \Pi^{(1)}(\beta,z)$$

$$\rho^2 k_B T \chi = \Pi^{(2)}(\beta,z)$$

where χ is the isothermal compressibility.

Consider now a small value of x, corresponding to a low temperature. Equation (A.31) says that if y is also small, i.e. $y<1$ (corresponding to a low activity) then ρ_n is an exponentially decreasing function. If $y=1$ then ρ_n decreases less fast. If $y>1$ then ρ_n exhibits a minimum. The value of n at which this minimum occurs is called n_c. For $n>n_c$ the number density diverges, so for

$x<1$ and $y>1$ there is a large probability to find a cluster of infinite size, indicating that the vapor has condensed to liquid. So the turning point $y=1$ can be identified as the saturation point.

Using $y=1$ in (A.29), z at the saturation point can be found. Since $z = e^{\beta\mu}/\Lambda^3$ an expression for the chemical potential μ at the saturation point can be derived.

$$\mu_{sat} = -E_0 - TS_0 + k_B T \ln \Lambda^3 \tag{A.32}$$

Now assume that y is slightly larger then 1, e.g. $y=1+\delta y$. Then $\mu-\mu_{sat}$ can be found after linearizing in δy.

$$\mu - \mu_{sat} = k_B T \ln\left(\frac{z}{z_{sat}}\right) \approx k_B T \delta y \tag{A.33}$$

Using the derivative of ρ_n the critical cluster size n_c can be expressed in terms of $\mu-\mu_{sat}$. The result yields [KAL95]

$$n_c = \left[\frac{a_0(w - \omega T)\sigma}{\mu - \mu_{sat}}\right]^{\frac{1}{1-\sigma}} \tag{A.34}$$

Since the size of a critical cluster decreases with temperature and the smallest critical cluster is given by $n_c=1$ and $0<\sigma<1$, the term between square brackets in (A.34) should always be larger or equal to 1. So there is a limiting temperature given by[1]

$$|\mu - \mu_{sat}| = a_0(w - \omega T) \tag{A.35}$$

So the maximum value of T allowed is given by $T = T_c = w/\omega$. This temperature is identified as the critical temperature, since condensation (and the formation of critical clusters) cannot take place for $T>T_c$.

Another useful result now emerges by introducing

[1] The restriction that $\mu-\mu_{sat}$ should always be positive follows from the restriction that the chemical potential should be real.

$$\gamma_{micro} = w\left(1 - \frac{T}{T_c}\right) \tag{A.36}$$

as the microscopic surface tension (an acceptable definition since at the critical point the surface tension should be zero). Equation (A.26) can no be written as

$$\frac{q_n}{V} = q_0 \Lambda^{3n} e^{-n\beta\mu_{sat}} e^{-a_0 n^{\sigma}\beta\gamma_{micro}} n^{-\tau} \tag{A.37}$$

indicating that the configuration integral is related to the chemical potential at the saturation point and the surface energy of the n-cluster. The only unknowns here are q_0, τ and γ_{micro}.

Now, assuming γ_{micro} is given by some model describing the microscopic surface tension, only q_0 and τ need to be known. Assume that assumptions made so far can be extended to the critical point, e.g. y=x=1. Then the equation of state at the critical point and the number density are given by

$$\begin{aligned} \frac{p_c}{k_B T_c} &= q_0 \zeta(\tau) \\ \rho_c &= q_0 \zeta(\tau - 1) \end{aligned} \tag{A.38}$$

where $\zeta(x)$ is the Riemann zeta function. So the critical compressibility factor $Z_c = p_c/\rho_c k_B T_c$ can now be expressed as a function of τ only.

$$Z_c = \frac{\zeta(\tau)}{\zeta(\tau - 1)} \tag{A.39}$$

Solving this equation yields τ. Since ρ_c is known for numerous substances it can be used in combination with the value of τ from equation (A.39) to solve q_0. With q_0 and τ known, the configuration integral is now known except for γ_{micro}.